

RNI: DELENG/2005/15153

Publication: 15th of every month

Posting: 19th/20th of every month at NDPSO

No: DL(E)-01/5079/17-19

Licensed to post without pre-payment U(E) 28/2017-19

Rs.150

ISSN 0973-2136

www.mycoordinates.org

Coordinates

Volume XIV, Issue 8, August 2018

THE MONTHLY MAGAZINE ON POSITIONING, NAVIGATION AND BEYOND

Clustering of Geo tectonic using GNSS data

Opportunities and use of Android GNSS Raw Measurements

Visit us at **INTERGEO 2018**

Frankfurt, Germany 16- 18 OCTOBER Hall 12.1 Booth 12.1D.023

Leica Pegasus:Two Ultimate Mobile Reality Capture

Digitisation of city infrastructures, planning, and resources is the foundation of the Smart City. The Pegasus:Two Ultimate will enable your growth and ability to offer the best solution for this market. Seamless 360° imagery calibrated to the digital point cloud will help you to deliver easily realised data assets.

Visit leica-geosystems.com/mobilemapping
for more information or to request a demo.



Leica Geosystems AG
leica-geosystems.com



- when it has to be **right**

Leica
Geosystems

©2018 Hexagon AB and/or its subsidiaries and affiliates.
Leica Geosystems is part of Hexagon. All rights reserved.

record • replay • simulate



LabSat3 WIDEBAND

The most powerful LabSat yet, the new **LabSat 3 WIDEBAND** captures and replays more GNSS signals at a much higher resolution than before.

Small, battery powered and with a removable solid state disk, **LabSat 3 WIDEBAND** allows you to quickly gather detailed, real world satellite data and replay these signals on your bench.

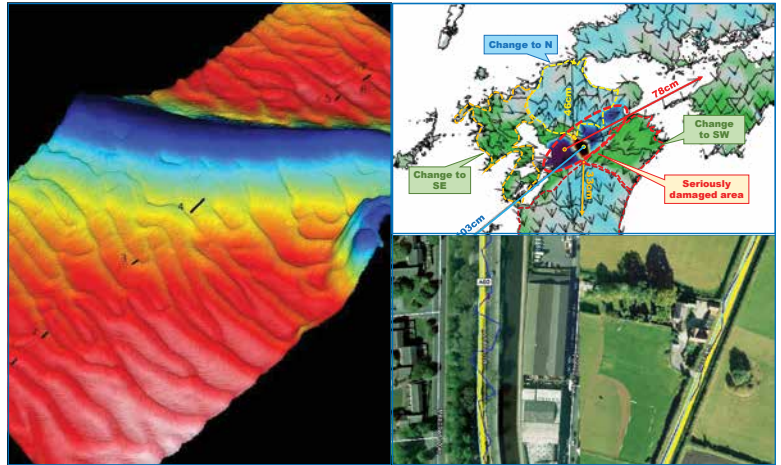
With three channels, a bandwidth of up to 56MHz and 6 bit sampling, **LabSat 3 WIDEBAND** can handle almost any combination of constellation and signal that exists today, with plenty of spare capacity for future planned signals.

LabSat 3 WIDEBAND can record and replay the following signals:

- GPS: L1 / L2 / L5
- GLONASS: L1 / L2 / L3
- BeiDou: B1 / B2 / B3
- QZSS: L1 / L2 / L5
- Galileo: E1 / E1a / E5a / E5b / E6
- SBAS: WAAS, EGNOS , GAGAN, MSAS, SDCM
- IRNSS



www.labsat.co.uk



In this issue

Coordinates Volume 14, Issue 08, August 2018

Articles

- Clustering of Geo-tectonics using GNSS data** SHUNJI MURAI AND HIDEO SUZUKI 7 **Detection of Pest Infestation Area in Paddy Field by Visible Bands Vegetation Indices** SITI NURFARHANA MD NOOR AND ABDUL RASHID MOHAMED SHARIFF 10 **Semi-buried seabed object detection: Sonar vs. Geophysical methods** DINO DRAGUN, LIESELOT NOPPE, PIERRE SERPE, EMELINE CARON, ASTRID ROBERT 15 **Geomagnetic Storms: Impact on GPS/GNSS signal delay over the low latitudes** K C T SWAMY, M A FARIDA AND E UPENDRANATH GOUD 20 **Opportunities and practical use of Android GNSS Raw Measurements** JUSTYNA REDELKIEWICZ, MARTIN SUNKEVIC, PAOLO CROSTA, MOISES NAVARRO-GALLARDO AND LUKASZ BONENBERG 39

Columns

- My Coordinates** EDITORIAL 6 **His Coordinates** STUART WOODS 40 **News** IMAGING 40 UAV 42 LBS & AUTONOMOUS DRIVING 43 GNSS 44 GIS 46 INDUSTRY 47 GALILEO UPDATE 48 **Mark your calendar** SEPTEMBER 2018 TO NOVEMBER 2018 50

This issue has been made possible by the support and good wishes of the following individuals and companies

Abdul Rashid Mohamed Shariff, Astrid Robert, Dino Dragan, Emeline Caron, E Upendranath Goud, Hideo Suzuki, Justyna Redelkiewicz, K C T Swamy, Lieselot Noppe, Lukasz Bonenberg M A Farida, Martin Sunkevic, Moises Navarro-Gallardo Paolo Crosta, Pierre Serpe, SitiNurfarhanaMd Noor, Shunji Murai and Stuart Woods and; Effigis, Hexagon, Javad, Labsat, NTLab, Pentax, Riegl, SBG System, and many others.

Mailing Address

A 002, Mansara Apartments
C 9, Vasundhara Enclave
Delhi 110 096, India.

Phones +91 11 42153861, 98102 33422, 98107 24567

Email

[information] talktous@mycoordinates.org

[editorial] bal@mycoordinates.org

[advertising] sam@mycoordinates.org

[subscriptions] iwant@mycoordinates.org

Web www.mycoordinates.org

Coordinates is an initiative of CMPL that aims to broaden the scope of positioning, navigation and related technologies.

CMPL does not necessarily subscribe to the views expressed by the authors in this magazine and may not be held liable for any losses caused directly or indirectly due to the information provided herein. © CMPL, 2018. Reprinting with permission is encouraged; contact the editor for details.

Annual subscription (12 issues)

[India] Rs.1,800 [Overseas] US\$100

Printed and published by Sanjay Malaviya on behalf of Coordinates Media Pvt Ltd

Published at A 002 Mansara Apartments, Vasundhara Enclave, Delhi 110096, India.

Printed at Thomson Press (India) Ltd, Mathura Road, Faridabad, India

Editor Bal Krishna

Owner Coordinates Media Pvt Ltd (CMPL)

This issue of Coordinates is of 52 pages, including cover.

Aiming at the future together!

PENTAX



D-600
Precise Aerial Imaging System
6 Rotor Multicopter with Autopilot



R-1500N & R-2800N
Reflectorless Total Stations
Total surveying solutions



W-1500N & W-2800
Windows CE Total Stations
Truly integrated systems



G6 Ti | Ni & G5
GNSS Receivers
Precision Satellite Surveying with wireless communications



S-3180V
Scanning System
3D laser measurement system

TI Asahi Co., Ltd.

International Sales Department
4-3-4 Ueno Iwatsuki-Ku, Saitama-Shi
Saitama, 339-0073 Japan

Tel.: +81-48-793-0118
Fax: +81-48-793-0128
E-mail: International@tiasahi.com

www.pentaxsurveying.com/en/

Authorized Distributor in India

Lawrence & Mayo Pvt. Ltd.
274, Dr. Dadabhai Naoroji Rd.
Mumbai 400 001 India

Tel.: +91 22 22 07 7440
Fax: +91 22 22 07 0048
E-mail: instmum@lawrenceandmayo.co.in

www.lawrenceandmayo.co.in



As a fallout of Brexit

It appears that the Public Regulated Services (PRS) of Galileo

Has become a contentious issue.

And similar to this, there are several other bones of contention...

Stakes are high

So is the pitch of stakeholders,

Hope it may not become messier in time to come

Galileo as a project had successfully

Endured many challenges earlier as well.

It is not simply a project,

It has been a celebration of collaboration among EU member nations

This spirit is worth emulating.

Bal Krishna, Editor
bal@mycoordinates.org

ADVISORS **Naser El-Sheimy** PEng, CRC Professor, Department of Geomatics Engineering, The University of Calgary Canada, **George Cho** Professor in GIS and the Law, University of Canberra, Australia, **Professor Abbas Rajabifard** Director, Centre for SDI and Land Administration, University of Melbourne, Australia, **Luiz Paulo Souto Fortes** PhD Associate Professor, University of State of Rio Janeiro (UERJ), Brazil, **John Hannah** Professor, School of Surveying, University of Otago, New Zealand

Clustering of Geo-tectonics using GNSS data

If comparisons are made between the newly defined dynamic geo-tectonic map and the existing geo-tectonic and fault maps, the new image map shows much better relations with the distribution of earthquakes



Prof. em. Dr. Shunji Murai
Chairman, Geo-tectonics Working Group (GEOTECWG), Japan Association of Remote Sensing, Chief

Technical Officer, Japan Earthquake Science Exploration Agency Co. Ltd., Chairman, Asian Association on Remote Sensing



Hideo Suzuki
Co-chairman, GEOTECWG, Japan Association of Remote Sensing, Professional geo-scientist, Aero Asahi Co. Ltd.

The existing geo-tectonic map of Japan has been produced by geological survey, rock classification, historical geological processes, faults etc. by expert geologists, geo-scientists, geographers and others. However, each geo-tectonic map may differ depending on by whom they were compiled. Dynamic changes in the three dimensional coordinates of GNSS data provide information about crustal movements of the earth, which could be classified into homogeneous crustal units. Since the authors assumed that such homogeneous units should be significantly related to the geo-tectonic maps or the distribution of large earthquakes, a clustering technique has been applied to weekly averaged GNSS data of about 1,000 Continuing Observing Reference Stations (CORSSs) all over Japan for the year of 2016. Astonishingly the clustering map determined from the GNSS data shows geo-tectonic structure which is highly correlated with the distribution of past large earthquakes.

Why clustering of geo-tectonics with GNSS data needed?

The reason for referring to the year of 2016 in this paper is that a large earthquake, namely “Kumamoto Earthquake”, occurred in Kumamoto Prefecture, Kyushu Island, Japan on the 16th April 2016 with M7.3 and Japanese seismic intensity level 7 (the maximum intensity). The quake created drastic horizontal as well as vertical changes in Kyushu Island (see Figure 1). The arrows show horizontal change in the green, yellow and red shaded areas as rising while light blue colors show sinking just after the earthquake. Looking at the figure carefully, certain areas move in similar directions while others in different directions as shown by the colored dotted lines in the figure. This behavior indicates that large areas consist of groups of different units of dynamic geo-tectonic structure. The authors have recognized that the geo-tectonic map should be based on geo-dynamism rather than static geological characteristics.

GNSS data and the clustering method used

GNSS data of the weekly average of X, Y and Z coordinates in a geo-centric coordinate system at 1,037 CORSSs in the year of 2016 (52 weeks) were selected for the clustering analysis. Those GNSS data can be downloaded free of charge from the homepage of Geo-spatial Information Authority (GSI), Japanese Government. In this research all software selected is open source, such as Ubuntu Linux, QGIS, R,

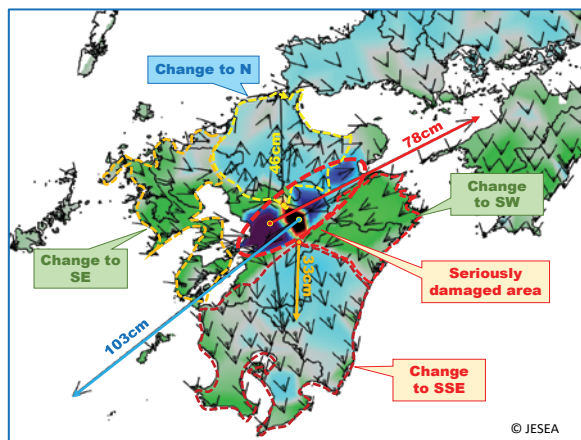


Figure 1: Horizontal and vertical change after Kumamoto Earthquake

Cloud Compare, Libre Office etc. Before applying the clustering method, we checked data characteristics such as variance and co-variance, principal components, correlation matrix and so on for the purpose of avoiding extremely abnormal points. A clustering method called “k-medoids” has been selected instead of “k-means” as it is more robust against large errors when included in clustering. The clustering of “k-medoids” can be chosen from the open source software for statistical analysis “R”.

components, which comprise a cumulative proportion of 96.7% of the variability of the data. Initially we classified the data into 6 clusters in the domain of principal components of all Japan Islands as shown in the left side of Figure 2, which revealed unusual distributions due to some extremely abnormal values. Then we tried clustering again without those extremely abnormal points in the same area, resulting in much better clustering distributions as shown in Figure 2(b) which comprised 98.1% cumulative variability.

Clustering of GNSS data

The clustering has been applied to the domain of the first and the second principal

The number of clusters selected in the clustering method should be compared with the existing geo-tectonic map with limited geo-tectonic classes. We

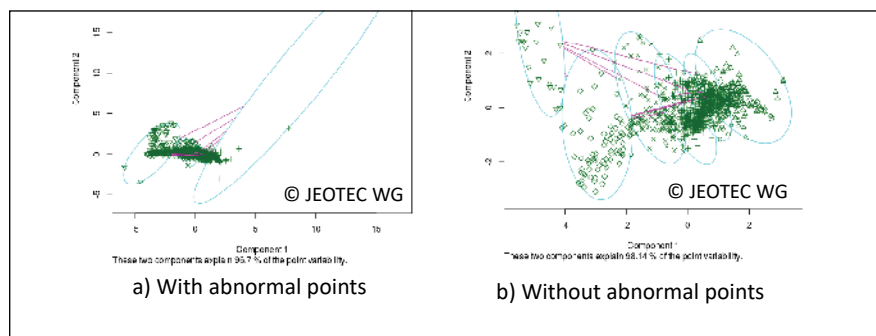


Figure 2: Clustering distributions with and without abnormal points

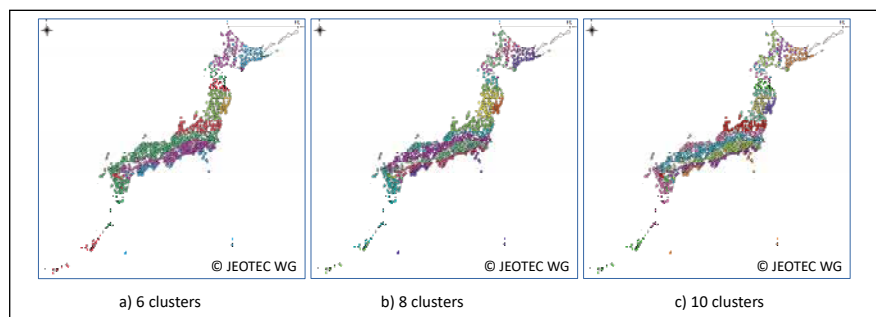


Figure 3: Clustering results with 6 to 10 clusters

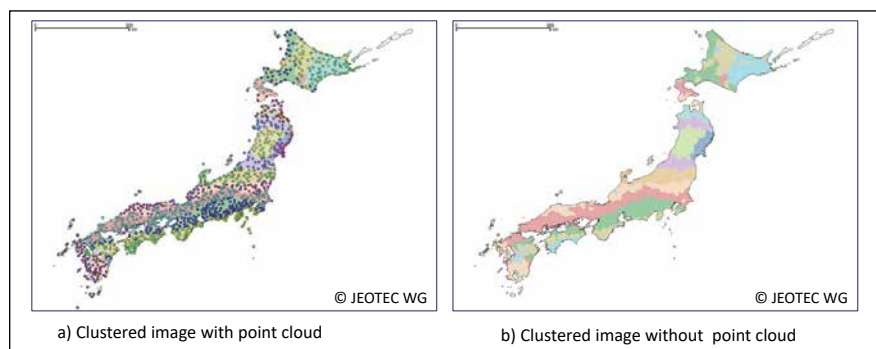


Figure 4: Clustering results with 10 clusters of all Japan Islands

tested from 6 to 10 clusters of all Japan Islands, out of which three cases of 6, 8 and 10 clusters are shown in Figure 3 in which the different colors mean different clusters. The authors judged that 10 clusters would be reasonable to compare with the existing geo-tectonic map.

For the purpose of comparison with the existing geo-tectonic map, the point cloud clustering map has been interpolated into a smooth image as shown in Figure 4 using a simple method of nearest neighbor to ensure quantitative repeatability can be guaranteed by other scientists.

Comparison of new geo-tectonic map with the existing geo-scientific map

It would be meaningless if a new geo-tectonic map were produced without scientific definitions that are comparable with existing scientific terminology.

Firstly we have compared the clustered image with the existing geo-tectonic map with major faults as recorded in a Japanese national atlas, with the distribution of past earthquakes larger than Japanese seismic intensity level 5 as shown in Figure 5. In the figure, the larger circles mean higher seismic intensity level, while color refers to the depth of earthquakes; yellow means less than 15 km, light blue between 15 and 30 km and blue deeper than 30 km.

The following observations have been obtained.

- Though some similarities are recognized in the two geo-tectonic maps, many parts are completely different. For example, the blue color zone in the existing map dominates central and northern Japan, but the newly clustered image map does not show such a dominant zone.
- Regarding the locations of earthquakes in the two maps, most that occurred inland are located near a boundary between two different clusters. However in the case of the existing geo-tectonic map, a strong relation between the location of earthquakes and the color zones or faults is not

found, although some earthquakes occurred around congested fault areas.

For a more detailed comparison, an enlarged area in north east Japan was selected showing detailed faults produced by National Institute of Advanced Science and Technology (AIST) and topography to check the relation between the clustered image map with the distribution of larger earthquakes, as shown in Figure 6 in which light red color lines refer to faults. The left hand map shows more clearly the relationship with the distribution of faults. The right hand side map is better for observing the topographic effect.

The following observations have been obtained.

- There are no significant relationships between the locations of faults and larger earthquakes, although there is a much higher relationship between the location of geo-tectonic boundaries and earthquakes.
- Concerning the relationship between the topography and earthquakes, we can say only that most earthquakes did not occur in the flat plains but in

hilly or mountainous areas. There is not a significant relationship between geo-tectonic zones and topography.

Finally the clustered image map is overlaid on the fault map in Figure 7 together with the distribution of the large Kumamoto Earthquakes which occurred in April 2016 including many aftershocks. The depth of Kumamoto Earthquakes was very shallow at about 10 km (yellow circles) which caused tremendous damage. Regarding the location of Kumamoto Earthquakes and faults, a belt of earthquakes is located much further north than the major fault belt zone. On the other hand, the distribution of Kumamoto Earthquakes is located near the boundaries between different clusters.

Conclusions

The variations of XYZ data derived by the GNSS CORSs during 2016 showed very interesting similarities in the clustered unit zones, which may be recognized as dynamic geo-tectonics. The clustering of geo-tectonics based on GNSS data derived from the CORSs

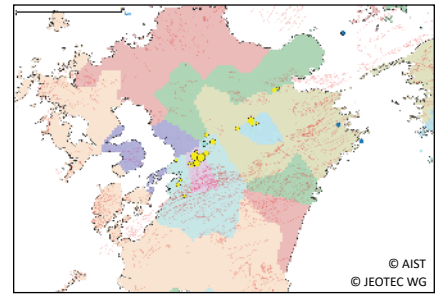


Figure7: Clustered image overlaid on fault map with large Kumamoto earthquakes in Kyushu, Japan


should be evaluated because the map derived is quantitative as well as repeatable. By contrast, the conventional geo-tectonic maps and geological maps have depended on experience and subjective judgement of geo-scientists.

If comparisons are made between the newly defined dynamic geo-tectonic map and the existing geo-tectonic and fault maps, the new image map shows much better relations with the distribution of earthquakes. It means that the dynamic geo-tectonic map would be much more useful for the prediction of earthquakes, as more than 70% of larger inland earthquakes occurred near the boundaries of the different clusters.

Acknowledgement

The authors appreciate Japan Association of Remote Sensing (JARS), Japan Earthquake Science Exploration Agency Co. Ltd. (JESEA) and Aero Asahi Co. Ltd. for their warm support of the research. The authors also thank Prof. John Trinder for his kind editing of the English paper.

References

- MURAI, S. and ARAKI, H: The prediction of Validation of Kumamoto Earthquake, Volume XII, Coordinates, July Issue 2016
- MURAI, S. and TESHIMA, S: Development of advanced earthquake prediction method using artificial intelligence, Volume XIV, Issue 3, March 2018 

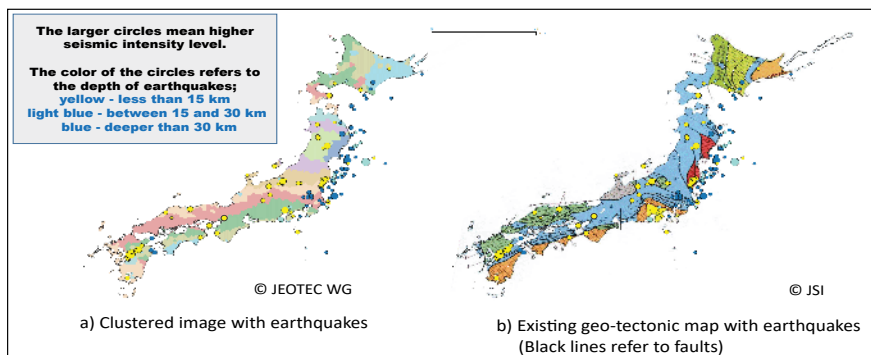


Figure 5: Comparison between clustered image and the existing Japan geo-tectonic map with the distribution of past larger earthquakes

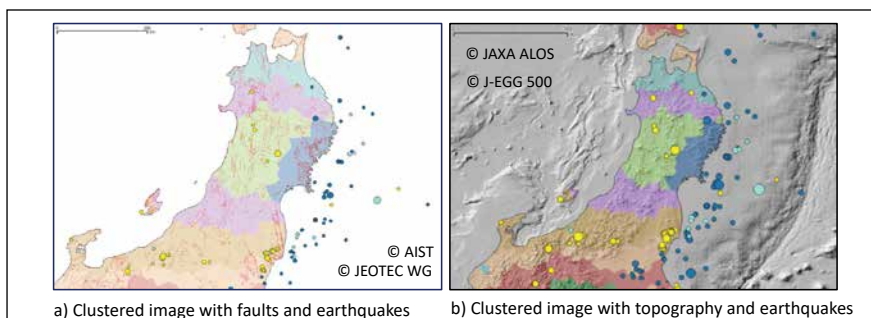


Figure 6: Clustered image overlaid on fault map and topographic map with the distribution of past larger earthquakes

Detection of pest infestation area by visible bands vegetation indices

This study investigates the ability of different vegetation indices in detection of pest infestation area from UAV-RGB images



Siti Nurfarhana Md Noor
Department of Biological and Agricultural Engineering, Faculty of Engineering, University of Putra, Malaysia



Abdul Rashid Mohamed Shariff
Department of Biological and Agricultural Engineering, Faculty of Engineering, University of Putra, Malaysia

Paddy is the third largest crop planted in Malaysia after oil palm and rubber. According to Paddy Statistics of Malaysia 2014 reported by Malaysian Department of Agriculture, nearly 679 239 hectares of land planted with paddy in Malaysia. There are certain agencies responsible for every cultivation area. These agencies manage the area from every aspect such as irrigation scheme, seeds selection, facilities development, pest and disease management, etc. Much research and attempts have been done in order to get an optimum yield and high quality of paddy in Malaysia, and efforts are ongoing.

However, due to the fact that almost every part of the plant can be consumed by pests at every stages of its growth, paddy field always being a target for various pests. This might reduce the quality and quantity of the yield. While pest control is one of the most critical operations in agriculture, farmers usually practice the traditional method of regular schedule based spraying even without any presence of pest in the field.

These chemicals kill useful insects which eradicate pests in crops (Johnny et al, 2014). In addition to that, chemicals are one of the main costs in agriculture activity. Regular spraying of pesticides might increase the cost of operation, including the cost of running the machinery and labor.

The idea of using remote sensing to determine pest infestation is to help detect the exact location of infested areas. Rather than regular spraying, applying the pesticide at the right time, in the right spot with an optimum amount

necessary to control the pest is another option that needs to be considered. To identify the type of pest infestation and determine the most effective and efficient way to control them is important. By using images taken from space, the exact spots of infestation can be detected. There are quite a number of researches done by using different means of remote sensing data and analysis.

However, the challenge is to use the most suitable means that convenient to the users from every aspect such as cost, area of field and availability of technology is important. Research on processing and analysing vegetation and spectral indices are widely done by using Near Infrared band and has useful results. However, installing near infrared sensor on UAV sensing is not so cost effective for small scale analysis.

This study investigates the ability of eight different vegetation indices in detection of Brown Plant Hopper's infestation area from UAV-RGB images. Four common visible bands vegetation indices were used and another four indices used are developed from manipulation and enhancement from the common indices.

The indices used are Vegetation Index Green (VIg), Vegetation Index Green (VARIG), Excess Green (ExG), Vegetation Visible Index (VVI), T1, T2, T3, and T4 where all of them are based on greenness where green area would yield higher index value than others. Thus, areas that have been injured by BPH will have lower index value than the areas not infested due to the hopper burn.

Materials and methods

UAV-RGB images

A field trip was done to fly the UAV at the study area and RGB images taken. A hexacopter UAV and Mission Planner Software was used for the work. Images were in Tagged Image File Format (TIFF) with a correct coordinate of the location as they have been georeferenced by the Department of Agriculture Kuala Lumpur. Table data acquisitions is shown in Table 1. The pest infestation areas in the images were confirmed by an officer from the Department of Agricultural Kuala Lumpur.

Study site

There are three different UAV images. The first study site is at a paddy field in Kampung Sungai Leman, Sekinchan. This area is located in Selangor and placed under Tanjung Karang irrigation Scheme area in Selangor. The other two images were obtained from Plant Biosecurity Division of Department of Agriculture, Kuala Lumpur. One of these images was acquired at FELCRA Kerian in Perak state and another one at Parit Haji Ali, Perak. There is only one lot for both sites in Sekinchan and Parit Haji Ali respectively, while there are 14 lots involved in the FELCRA study plot

All of these three sites practice similar activity that is paddy cultivation. Paddy was cultivated on these sites due to the suitability of the soil, weather, facilities and irrigation system.

UAV image pre-processing

Some basic pre-processing techniques were done for this study including mosaicking, georeferencing and clipping. All the steps of building an orthoimage from UAV images are processed by using AgisoftPhotoScan Professional and saved in the format of TIFF. Georeferencing the image enable in determination of exact location of the image. The image was georeferenced by using Georeference function in QGIS by inserting reference coordinate to four different points of

the image. The projection use for the image is WGS 1984 UTM 47 N. The orthoimage not only covered the area of study but also some other features. As this study focus on paddy, the image clipping is needed to ensure the vegetation indices calculated for only the paddy feature in the study area is calculated. Calculating the whole image would affect the calculation as vegetation indices calculated based on average area.

The images were clipped by using Raster Clip function in QGIS.

Application of Vegetation Indices

The indices used visible bands (Blue, Green, and Red) as the orthoimage is in visible bands. Four common indices were used while another four indices are computed especially for this study to test and compare the performance and

Table 1.: Visible Band Vegetation Indices

| No. | Index | Formulation (Band) |
|-----|--------------------------------|---|
| 1. | Vegetation Index Green (VIg) | $(GREEN-RED) / (GREEN+RED)$ |
| 2. | Vegetation Index Green (VARig) | $(GREEN-RED)/(GREEN+RED-BLUE)$ |
| 3. | Excess Green (ExG) | $2GREEN-RED-BLUE$ Where; GREEN= $GREEN/RED+GREEN+BLUE$ RED = $RED/ RED+GREEN+BLUE$ BLUE = $BLUE/RED+GREEN+BLUE$ |
| 4. | Vegetation Visible Index (VVI) | $[[(1- (R-RO))/(R+RO)) \times [(1- (G-GO)) / (G+GO)) \times [(1- (B-BO))/(B+BO))]] ^{1/w}$ Where; RGBo= (40,60,10) and w=1 |
| 5. | T1 | $(2GREEN-RED-BLUE) / (GREEN+RED-BLUE)$ |
| 6. | T2 | $(GREEN-RED-BLUE) / (GREEN+RED+BLUE)$ |
| 7. | T3 | $(2GREEN-RED) / (GREEN+RED)$ |
| 8. | T4 | $(GREEN / GREEN+RED+BLUE) - (RED / GREEN+RED+BLUE)$ |

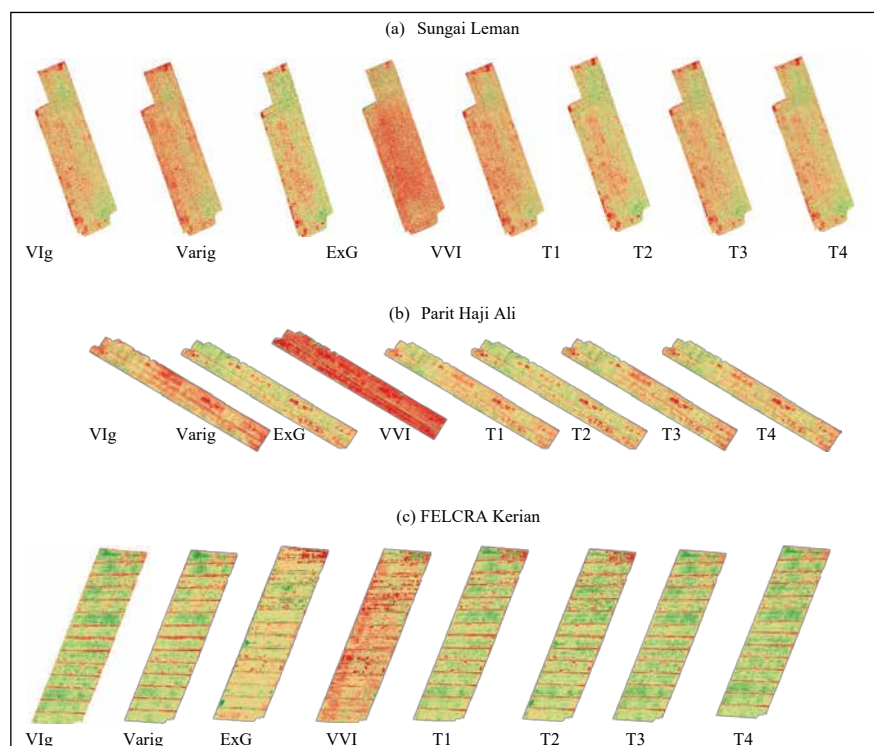


Figure 1. Vegetation Indices Images for Three Locations

The vegetation indices have been computed on three different images with different locations and sizes.

The algorithm converted multiband raster image into a single band raster image. The results are in colour gradient that emphasise the value of index where greener area has bigger index values and vice versa

emphasise the value of index where greener area has bigger index values and vice versa as shown in Figure 1 (a),(b), and (c).

By visualizing the output, it can be concluded that some indices were able to show greenness by showing obvious colour contrast while some were not. The original images were in monochrome where the gradient is from black to white. Images shows colour gradient from green to red where dark green shows high index value and red is for low index value. When paddy is infested by pest, the plant will usually die or suffer some distortion. The leaves will not be as green as the healthy and non-infested plant and in most serious cases the leaves will be in brown, red or white colour. This is where these indices are practical as the infested area will have low index value as they have lower green reflectance value. The images where compared to the original RGB images to validate the exact location of the infested areas.

From the four common indices, the images that produce most colour contrast are the VIg index. This index was able to shows green area more than the others. However, the infested area does not really contra in the images by VIg compared to the images produce by ExG index. ExG index was able to shows the infested area more clearly than the other indices. The formula of ExG where the green band reflectance intensity is doubled before subtracting the other bands reflectance intensity values is the factor of the results.

From the testing indices, T1,T2, T3, and T4, index that produce the most contrast image in terms of greenness index T1 while the index that was able to show the most contrast in terms of infested area was index T2. T1 is the manipulation of ExG index's formula by changing the normalization equation. Figure 2 shows the comparison between images of ExG index and T1 index at FELCRA Kerian. It can be seen in the Figure 2 the images of ExG and T1 index is about the same, only in T1 the greenness are greater contrast.

T2 index is the manipulation of VARIg index. Instead of only subtracting Red intensity values from Green values,

capability. All the listed Vegetation Indies with formulation used in this study are listed in Table 1. The equations of each index are different hence, the computed result should be different as the reflectance value for each bands is different. As all indices used are based on greenness, the main concept is to eliminate other reflectance values from Green reflectance. The same concept is used for the four Testing Indices. These indices formulated by manipulation and enhancement of the common indices. T1 is an index inspired by ExG with manipulation of normalization equation while T2 was inspired by VARIg index with addition of Blue reflectance value to be subtracted from Green and to be added for normalization equation.

T3 and T4 indices both inspired from VIg index. The index computations were done by using Raster Calculation tool in QGIS. This tool basically calculates the single value of indices by running the formulation and convert multiband raster to single band vegetation indices.

Image analysis

The image produced were analysed visually and statistically. From visual, the colour contrast of the images was compared for all index images. Analysis was done by computing statistical data of every single band vegetation indices raster. The min, max, mean and standard deviation of each raster were tabulated and graph of statistical distribution was plotted. The values were then compared in order to conclude the stability, performance and capability of the index in the detection of infestation area by brown plant hopper.

Result and discussion

Visual comparisons of vegetation indices images

The vegetation indices have been computed on three different images with different locations and sizes. The algorithm converted multiband raster image into a single band raster image. The results are in colour gradient that

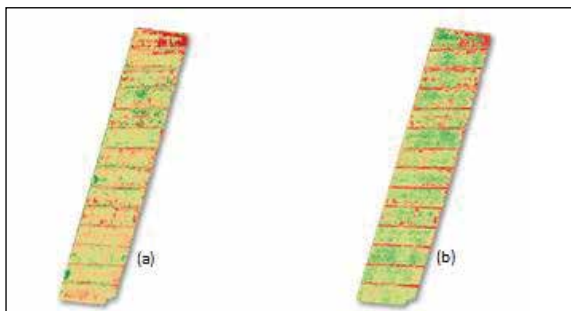


Figure 2. Comparison of Images between (a) ExG Index and (b) T1 Index

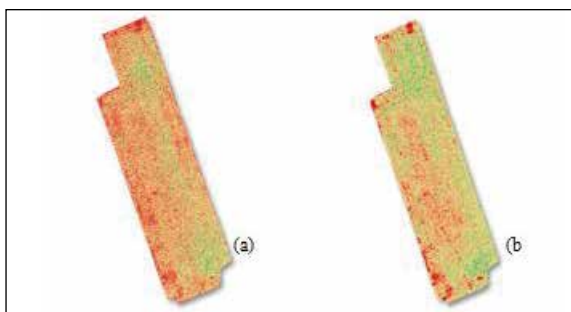


Figure 3. Comparison of Images between (a) VARIg Index and (b) T2 Index

the Blue band intensity values was also subtracted. Figure 3 shows the comparison between images of T2 index and VARlg index at Sungai Leman. From the figure, T2 index image shows more contrast in greenness and infested area compared to VARlg index image.

Image analysis

The statistical distribution of the images varies not only when compared to

Table 2. Statistical Distribution of Vegetation Indices Images for Three Location; (a) Sungai Leman, (b) Parit haji Ali and (c) FELCRA Kerian

| | Min | Max | Mean | STDV |
|-------|--------|--------|--------|-------|
| Vig | 0.213 | 0.589 | 0.367 | 0.090 |
| VARlg | 0.494 | 1.875 | 0.977 | 0.338 |
| ExG | 0.148 | 0.424 | 0.270 | 0.066 |
| VVI | 0.016 | 0.077 | 0.033 | 0.015 |
| T1 | 0.576 | 2.211 | 1.158 | 0.398 |
| T2 | -0.234 | -0.050 | -0.153 | 0.044 |
| T3 | 0.820 | 1.384 | 0.135 | 0.135 |
| T4 | 0.136 | 0.351 | 0.227 | 0.052 |

(a)

| | Min | Max | Mean | STDV |
|-------|--------|--------|--------|-------|
| Vig | 0.060 | 0.373 | 0.241 | 0.076 |
| VARlg | 0.130 | 1.016 | 0.600 | 0.213 |
| ExG | 0.436 | 0.658 | 0.537 | 0.049 |
| VVI | 0.024 | 0.104 | 0.052 | 0.083 |
| T1 | 0.094 | 1.160 | 0.670 | 0.266 |
| T2 | -0.315 | -0.141 | -0.220 | 0.043 |
| T3 | 0.589 | 1.060 | 0.862 | 0.114 |
| T4 | 0.039 | 0.231 | 0.151 | 0.047 |

(b)

| | Min | Max | Mean | STDV |
|-------|--------|--------|--------|-------|
| Vig | 0.187 | 0.636 | 0.369 | 0.105 |
| VARlg | 0.481 | 2.641 | 1.010 | 0.895 |
| ExG | 0.105 | 0.468 | 0.273 | 0.082 |
| VVI | 0.024 | 0.352 | 0.161 | 0.082 |
| T1 | 0.278 | 2.474 | 1.187 | 0.874 |
| T2 | -0.263 | -0.021 | -0.152 | 0.055 |
| T3 | 0.780 | 1.454 | 1.053 | 0.157 |
| T4 | 0.117 | 0.375 | 0.228 | 0.060 |

(c)

different vegetation indices but also varies when comparing the same indices for different locations (Table 2).

For Sungai Leman, the three indices that have the smallest standard deviation are VVI, T2 and T4 indices with the range of 0.015-0.052 which is the closest to 0 and also a very small mean different. Small standard deviation shows that the data points are very close to the mean value or the expected value. It's different for data from FELCRA Kerian and Parit Haji Ali Vegetation Indices images. The indices that have the lowest standard deviation are T2, T4 and ExG with the range of 0.043 – 0.082.

Indices T2, T4, ExG and VVI shows the smallest mean differences and standard deviations when compared to the others.

The indices mean and standard deviations were compared in Table 3. The difference in means and standard deviations for T2 index is the smallest when compared with the other three indices. Another index that has a difference in mean and standard deviation values less than 0.1 is T4 index. Figure 4 shows the distribution comparison between the four indices within these study areas. The distribution of indices T2 and T4 seems more stable than the other two indices. The maximum and minimum values are almost the same for all three locations.

T2 and T4 indices show most stability and reliability as they have the smallest value in standard deviation and smallest difference of mean values. By comparing statistical distribution for the three locations, the stability of the indices can

Table 3. Comparisons of Mean and Standard Deviation for Index T2, T4, ExG and VVI

| | Sungai Leman | | FELCRA Kerian | | Parit Haji Ali | |
|-----|--------------|-------|---------------|-------|----------------|-------|
| | Mean | STDV | Mean | STDV | Mean | STDV |
| T2 | -0.153 | 0.044 | -0.220 | 0.043 | -0.152 | 0.055 |
| T4 | 0.227 | 0.052 | 0.151 | 0.047 | 0.228 | 0.060 |
| ExG | 0.270 | 0.066 | 0.537 | 0.049 | 0.273 | 0.082 |
| VVI | 0.033 | 0.015 | 0.052 | 0.083 | 0.161 | 0.082 |

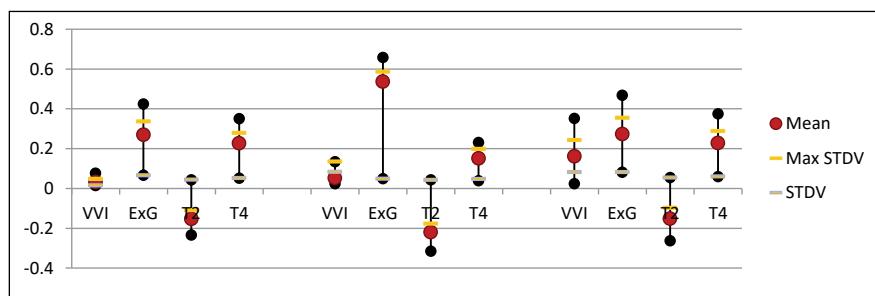


Figure 4. Statistical Distribution of Index T2, T4, ExG and VVI for Three Locations

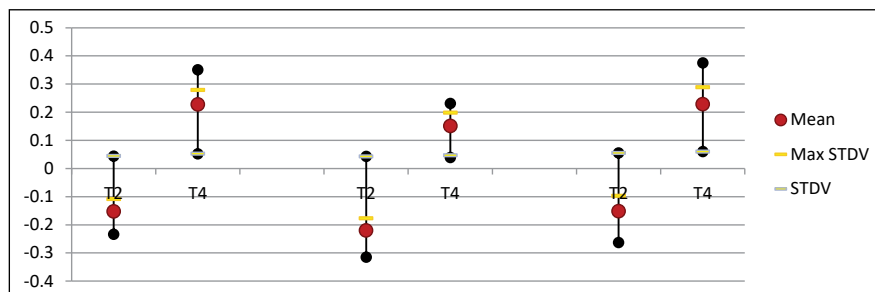


Figure 5. Statistical Distribution of Index T2 and T4

be seen (Figure 5). Even though both indices show stability, T4 is more stable and reliable in the detection of Brown Plant Hopper infestation area in paddy fields in the study areas in Malaysia.

Conclusion


Indices T2 and T4 were able to show the infestation area clearly by producing images that have more colour contrast. A comparison between T2 and T4 indices showed both indices to have stability. However, T4 is more reliable due to smaller value of standard deviation. The research contributes the new index T4 to aid detection of paddy infestation using RGB images. This work will benefit the paddy cultivation industry.

Acknowledgement

The authors would like to thank to Plant Biosecurity Division Department of Agriculture, Kuala Lumpur for their willingness to share their data that helped in successful completion of this research. MOSTI Science Fund Research grant 06-01-04-SF2371 is duly acknowledged.

References

- Bokusheva, R., Kogan, F., Vitkovskaya, I., Conradt, S., & Batyrbayeva, M. (2016). Satellite-based vegetation health indices as a criteria for insuring against drought-related yield losses. *Agricultural and Forest Meteorology*, 220, 200–206. <https://doi.org/10.1016/j.agrformet.2015.12.066>
- Dyck, V. A., Misra, B. C., Alam, S., Chen, C. N., Hsieh, C. Y., & Rejesus, R. S. (1979). Ecology of the brown planthopper in the tropics. *International Rice Research Institute: Brown Planthopper: Threat to Rice Production in Asia.*, 61–98.
- Hunt, E. R., Doraiswamy, P. C., McMurtrey, J. E., Daughtry, C. S. T., Perry, E. M., & Akhmedov, B. (2012). A visible band index for remote sensing leaf chlorophyll content at the Canopy scale. *International Journal of Applied Earth Observation and Geoinformation*, 21(1), 103–112. <https://doi.org/10.1016/j.jag.2012.07.020>
- Motohka, T., Nasahara, K. N., Oguma, H., & Tsuchida, S. (2010). Applicability of Green-Red Vegetation Index for remote sensing of vegetation phenology. *Remote Sensing*, 2(10), 2369–2387. <https://doi.org/10.3390/rs2102369>
- Mróz, M., & Sobieraj, A. (2004). Comparison of several vegetation indices calculated on the basis of a seasonal SPOT XS time series, and their suitability for land cover and agricultural crop identification. *Technical Sciences*, 7(7), 39–66. <https://doi.org/10.1080/10106040608542399>
- Ponti, M. P. (2013). Segmentation of low-cost remote sensing images combining vegetation indices and mean shift. *IEEE Geoscience and Remote Sensing Letters*, 10(1), 67–70. <https://doi.org/10.1109/LGRS.2012.2193113>
- Rabatel, G., Gorretta, N., Labb, S., Rabatel, G., Gorretta, N., & Labb, S. (2011). Getting NDVI spectral bands from a single standard RGB digital camera : a methodological approach e To cite this version : Getting NDVI Spectral Bands from a Single Standard RGB Digital Camera : 14th Conference of the Spanish Association for Artificial Intelligence, 333–342. Retrieved from <https://hal.archives-ouvertes.fr/hal-00648439/document>
- Red, N. (2006). List of Vegetation Spectral Indices References Baret , F ., G . Guyot , and D . Major .1989 . TSAVI : a vegetation index which minimizes soil brightness effects on LAI and APAR estimation . 12 th Canadian Symposium on Remote Sensing and IGARSS '90 , p . *Remote Sensing of Environment*, 1994–1996.
- Reid, A. M., Chapman, W. K., Prescott, C. E., & Nijland, W. (2016). Using excess greenness and green chromatic coordinate colour indices from aerial images to assess lodgepole pine vigour, mortality and disease occurrence. *Forest Ecology and Management*, 374, 146–153. <https://doi.org/10.1016/j.foreco.2016.05.006>
- Viña, A., Gitelson, A. A., Nguy-Robertson, A. L., & Peng, Y. (2011). Comparison of different vegetation indices for the remote assessment of green leaf area index of crops. *Remote Sensing of Environment*, 115(12), 3468–3478. <https://doi.org/10.1016/j.rse.2011.08.010>
- Xu, Y., Ou, J., He, H., Zhang, X., & Mills, J. (2016). Mosaicking of Unmanned Aerial Vehicle imagery in the absence of camera poses. *Remote Sensing*, 8(3). <https://doi.org/10.3390/rs8030204>
- Yahyanejad, S. (2013). Orthorectified Mosaicking of Images from Small-scale Unmanned Aerial Vehicles DISSERTATION, (March 2013), 88.
- Zheng, Y. L., Xu, L., Wu, J. C., Liu, J. L., & Duanmu, H. L. (2007). Time of occurrence of hopperburn symptom on rice following root and leaf cutting and fertilizer application with brown planthopper, *Nilaparvatalugens* (st??l) infestation. *Crop Protection*, 26(2), 66–72. <https://doi.org/10.1016/j.cropro.2006.04.001>
- Li, P., Jiang, L., & Feng, Z. (2013). Cross-comparison of vegetation indices derived from landsat-7 enhanced thematic mapper plus (ETM+) and landsat-8 operational land imager (OLI) sensors. *Remote Sensing*, 6(1), 310–329. <https://doi.org/10.3390/rs6010310>

The paper was presented at Asian Conference on Remote Sensing, Delhi, India October 23-27, 2017 

Semi-buried seabed object detection: Sonar vs. Geophysical methods

This paper deals with the site investigation processes of detecting a semi-buried object using multibeam echosounder, sidescan sonar and magnetometer data

Dino Dragun
GEOxyz, Belgium

Lieselot Noppe
GEOxyz, Belgium

Pierre Serpe
GEOxyz, Belgium

Emeline Caron
GEOxyz, France

Astrid Robert
GEOxyz, France

The purpose of this paper is to conduct the evaluation of the object detection using sonar and geophysical methods. Increasing interest in maritime archaeology has led to a growing need for measuring techniques or innovative methods for detecting and identifying underwater objects. Object detection usually consists of two steps: feature detection and classification. In the feature detection step, the relevant features of the object to be detected are gathered. Here is the definition of the feature provided by The International Hydrographic Organization (IHO). Standards for Hydrographic Surveys Special Publication 44 (IHO S-44) defines a feature as 'any object, whether manmade or not, projecting above the sea floor, which may be a danger for surface navigation'. Moreover, 'S-44 sets minimum standards for surveys conducted for the safety of surface navigation' and considers it the 'responsibility of each national authority to determine the precise characteristics of features to be detected'. Detection of objects occurs not only in the safety of navigation purpose, since finding such objects is the subject of interest for a wide group of professionals, including archaeologists, offshore construction specialists, and the military responsible for defending coastal waters. Challenge faced in this paper is detection of the semi-buried object, where we need to combine few survey methods in order to obtain reliable output results.

After first site investigation of the zone, sonar methods have been used only.

When data interpretation has been done, it was clear that object has been partly buried under the seabed. Since there was a strong indication that object is cable, it has been decided to involve marine magnetic technique (magnetometer) in next investigation, since the primary use of the magnetometer survey (geophysical method) is to provide evidence of the existence of ferrous material on or below the seabed. Due to the disturbance of the surrounding structure, marine magnetic survey gave less information than expected. Therefore, results of the site investigation have been interpreted mostly using sonar survey methods, especially sidescan sonar survey data.



Figure 1. Survey equipment used (from top to bottom order): Edgetech sidescan sonar Edgetech 4200, Multibeam echosounder Kongsberg EM3002 dual head, Magnetometer Geometrics G-882

Survey methods used for site investigation

Sonar and geophysical survey methods have been used during the survey. Purpose of sonar methods is to determine depths and detect object on the seabed, while geophysical method has been used to give the information about ferrous object under the seabed level.

Sonar survey methods

Sonar (Sound Navigation and Ranging) uses sound waves to find and identify objects in the water and determine bathymetry. There is a wide range of acoustic imaging systems including multibeam echosounders, sidescan sonar, single-beam echosounders, interferometric systems and sub-bottom profilers. Since aim of this site investigation was to get results about bathymetry and object at the seabed, multibeam echosounder and sidescan sonar have been used during the survey. Data interpretation analysis has been performed using multibeam bathymetry and multibeam and sidescan sonar backscatter data.

Both multibeam echosounders and sidescan sonars can be used to collect acoustic backscatter data, the data obtained from the reflection of acoustic energy back toward a sonar device, where its intensity can be measured. With multibeam backscatter, there are no shadows because the sonar head is on the vessel's hull and looking down over objects from a higher angle, instead of from one side or another. The high degree of bathymetric resolution and complete 3D coverage offered by these swath-sounding techniques is providing precise insights into complex sea floor geology and also allowing evaluations of dynamic sediment movements.

After various corrections are applied to the data, backscatter intensity is essentially a function of the seafloor's physical properties, namely acoustic impedance, roughness (grain-size and small-scale topography) and volume inhomogeneity (variability in the thin layer of sediment penetrated by the acoustic signal).

Sidescan imagery is less prone to be affected by the slope of the seafloor as it can be positioned, whereas the multibeam can only receive the backscatter intensity as it reaches the survey vessel.

Sidescan sonars and multibeam echosounders both collect acoustic backscatter that can be interpreted to represent variations in seabed materials. Sidescan sonar systems are specifically designed for this purpose, whereas most multibeam echosounder systems that are presently in operation in connection with oil industry activities were designed to collect very accurate bathymetry, with backscatter data being a byproduct of the soundings. Conventional sidescan sonar systems (excluding more sophisticated systems, such as those that use interferometry, beam forming and synthetic aperture technology) do not measure water depth, but the images contain indirect bathymetric information in the form of an increase in backscatter when the seafloor slopes toward the sonar and a decrease in backscatter when the seafloor slopes away from it. The result is 'acoustic shadows' behind features with relief relative to their surroundings.

Since object at the seabed is cable, the size of which is not so significant, especially height, there is presumption that cable will be seen only after sidescan sonar acquisition post processing.

Geophysical methods

Of the various geophysical technologies used for seabed mapping, the magnetic method has proved to be the most effective for locating ferromagnetic objects masked by sea floor sediments, buried under the seabed or on the seabed surface itself. Important parameters to detect semi-buried cable using this method are its radius of ferrous emission and altitude of the

magnetometer above the seabed during the acquisition. It is very difficult to detect underwater pipeline by conventional method, such as echo sounding and sidescan sonar method. Furthermore, the conventional acoustic methods cannot effectively detect seabed cable because the seabed cable is thin in size and often buried by sediments. On the contrary, the electromagnetic characteristics of seabed cable provide the possibility of detection by magnetism methods.

The ferromagnetic substance of seabed cable and the electrical current can produce an external magnetic field, its magnetic anomaly intensity (ΔT) is about 0.5-150 nT. Because the sensitivity of high resolution cesium vapor magnetometer can reach 0.005 nT (sampling rates at 1 Hz), the tiny change of magnetic anomaly produced by seabed cable can be effectively detected. Based on the characteristics of the magnetic field, the feature of the magnetic anomaly can be applied to analyze and identify seabed cable.

The detection limits are represented in the figure below. An object which is situated above 'curve 1' will always be detected. An object which is positioned below 'curve 2' will not be detected.

Maximum detection depth of ferromagnetic objects, assuming an average magnetic susceptibility:

curve 1: anomaly threshold of 5nT (worst conditions),

curve 2: anomaly threshold of 1nT (ideal conditions).

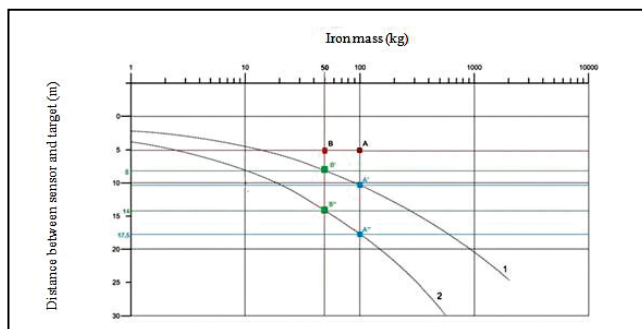


Figure 2. Diagram for detecting limits of iron mass versus distance between magnetometer sensor and target

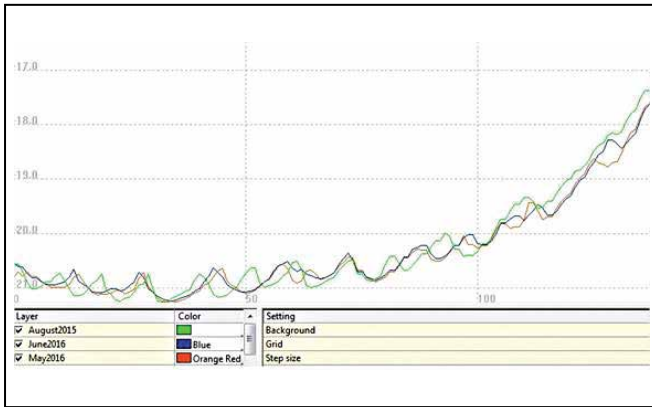


Figure 3 Overall crossprofile of the bathymetric data along the detected semi-buried cable between the first survey done in August 2015 and the second survey done in May/June 2016

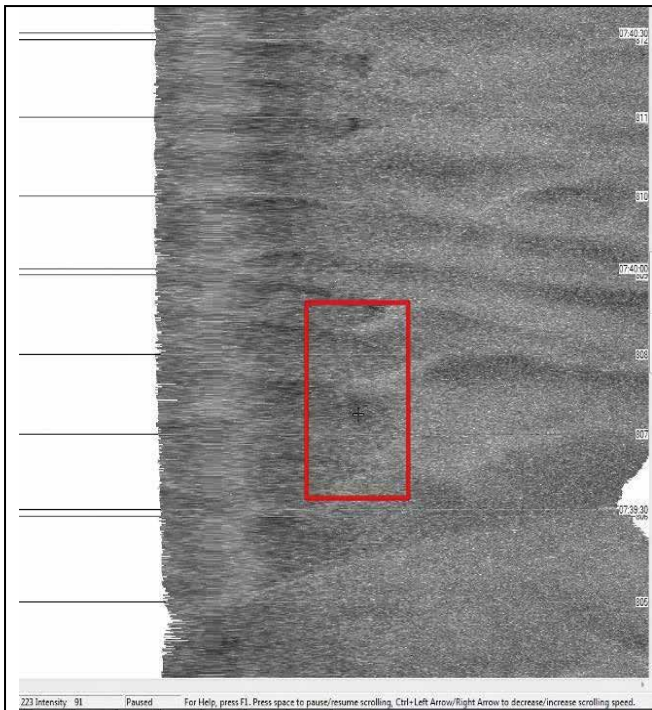


Figure 4. Multibeam backscatter data – red rectangle shows a location where cable section has been detected interpreting sidescan sonar data

Survey and methodology

Before each survey all the calibrations have been done (position verification, gyro check, absolute elevation check, multibeam patch test, sidescan sonar rub and wet test, USBL calibration). HiPAP 351P portable transducer for high precision acoustic positioning and underwater navigation has been used for the sidescan sonar and magnetometer positioning during this site investigation. Time difference between first and second site investigation survey is one year. After first survey when sonar methods (multibeam and sidescan sonar) were used, cable has been detected on several spots, only with sidescan sonar output results. Term 'Theoretical

position' has been used for the cable's detected position during first survey. Analyzing output results, cable sections were visible only on sidescan sonar which led to conclusion that cable has been semi-buried. Another survey method had to be included in the investigation, and since interest was to determine cable section under the seabed, geophysical survey method was a logic solution.

Multibeam survey

Kongsberg EM3002 dualhead provided primary bathymetric information at the survey location. In addition, as mentioned above, backscatter data has been recorded.

Multibeam survey has been executed on and around the theoretical position of the cable. No clear indications of the presence of the cable could be obtained. In post-processing, data has been double checked in 3D view to see if any linear irregularity became visible. Nothing could be found analyzing multibeam data which could indicate the cable presence.

Additionally, multibeam data from the first survey has been compared with the processed data from the second one. When checking the cross profiles we can see that the general maximum depth (between the ripple marks) is slightly shallower in most recent survey (approx. 5cm). The sand ripple marks are little smaller in second site investigation, and have moved along the seafloor.

As multibeam systems acquire both bathymetry (depth) and backscatter (intensity) data, backscatter data has been post processed and no indications of the cable sections presence have been found. The reason of not detecting semi-buried cable using multibeam data is mainly cable dimension, while sonar method is not most suitable one for cable detection in general. On the figure below there is an example of the location where cable section has been detected interpreting sidescan sonar data. No semi-buried cable section was visible interpreting multibeam backscatter data.

Sidescan sonar

Edgetech 4200 sidescan sonar has been used during the survey. Towed behind the vessel on average distance of 80m. Since sidescan sonar range was 75m, average altitude of the towfish was 7 meters, while total coverage was 200%. The high-resolution imaging of underwater environments afforded by sonar has proven particularly useful for the detection of objects on the seabed. During post processing procedure, all the cable sections have been double detected. As explained before, sidescan sonar has established itself as the predominant tool for imaging the ocean floor, giving good object detection and seabed character discrimination (Blondel and Murton, 1997). USBL calibration has been performed, to ensure correct positioning of the sidescan sonar and magnetometer system, while position accuracy after calibration is ± 1.5 m. The sidescan sonar data positioning is also checked during the post processing by

comparing the multibeam data with the mosaic from the SSS. On the latest survey we were able to locate the cable outcropping seven times at different locations as seen on the following figures:

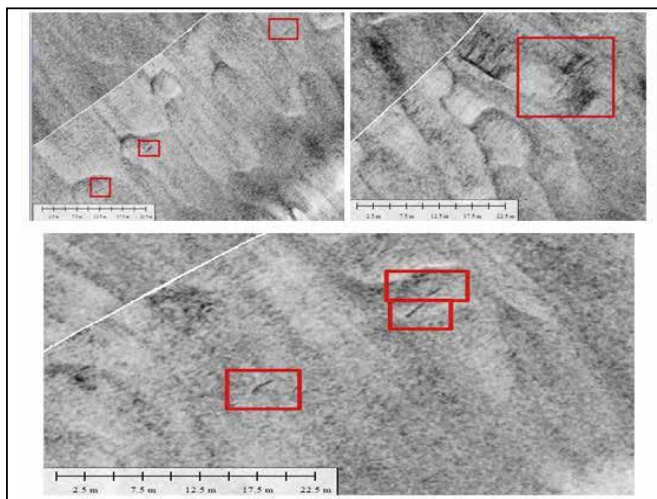


Figure 5. Red rectangles show location where cable section has been detected interpreting sidescan sonar data from most recent survey

Magnetometer survey

Geometrics model G-882 marine magnetometer was used to precisely measure the Earth's magnetic field. Magnetometer has been towed behind the sidescan sonar towfish with layback of 10 meters. To eliminate the magnetic effect of the survey vessel, the magnetometer sensor is towed behind the boat at a sufficient distance of about 4 times the vessel's length. During the magnetometer survey we had data interference due to the large structure presence nearby. According to it, there were no significant changes in the magnetic field which can indicate presence of the semi-buried cable. Indeed, on the following figure no variations appear on the signal detected from the large structure.

We can see the changes in magnetic field from 48861 nT to 48686 nT, which is 175 nT. It has been expected to see on this amplitude caused by nearby structure, change in the magnetic field which indicates cable presence, but interference with the structure is too strong, even at 200m distance, as shown in the figure below.

A strong filter has been applied to the data, to try to remove the influence of the structures. However, this didn't give any reliable and useful result.

Sonar vs. geophysical survey

Final results of the site investigation were not expected. Since aim of backscatter data, especially sidescan sonar, is to give information about objects on the seabed surface, while the primary use of the magnetometer is to provide evidence of the existence of ferrous material on or below the seabed.

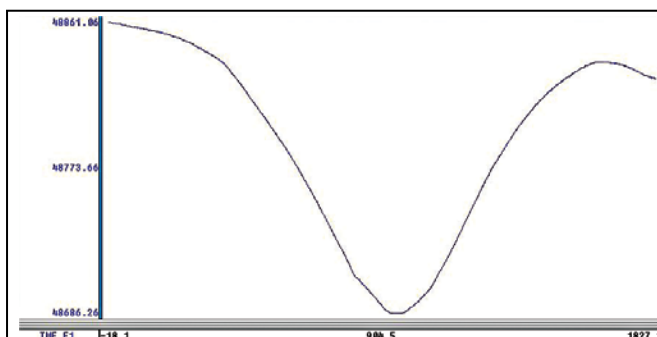


Figure 6. Example of data acquired by magnetometer along complete line (1.8km long) – huge magnetic field change due to the large structure nearby, x- axis: length of the survey line (m), y-axis: magnetic field (nT)

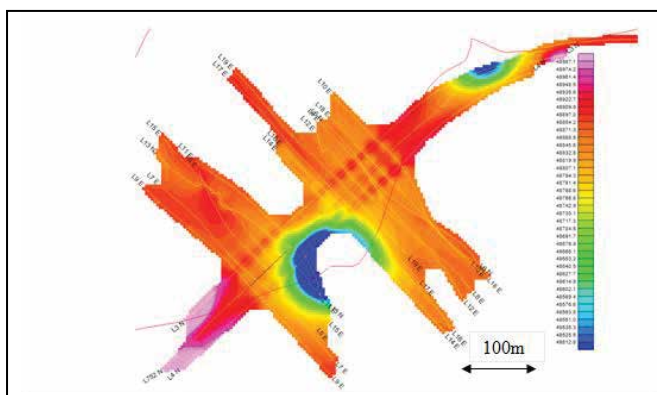


Figure 7. Gridding of the magnetic signal around semi-buried cable; values in nT. Black line: Theoretical position of the semi-buried cable.

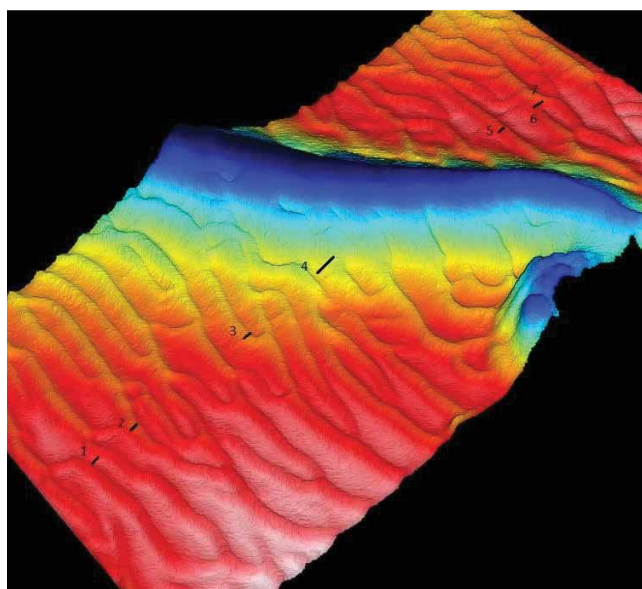


Figure 8. Bathymetric 3D detail view overlapped with semi-buried cable sections detected using sidescan sonar data from latest survey

Various maritime survey methods, such as sonar, optical and magnetic technologies, are used for locating submerged artifacts. Marine magnetic surveys have been successfully used for mapping marine ferrous targets, for magnetic mapping of contaminated seabed sediments, and for mapping archeological structures. Of the various technologies used for seabed mapping, the magnetic method has proved to be the most effective for locating ferromagnetic objects masked by sea floor sediments or buried under the seabed. Because the intensity of the magnetic field produced by a magnetized body drops rapidly as the distance to the measured point increases, tow fish configuration is widely used. There are, however, situations where the offshore structure in the survey area prevents the magnetometer survey to produce desired data, like during this investigation. Therefore, data interpretation had to rely on sonar methods, which provided enough information about cable exposure, length, cable sections, but not the total length and position which was the primary purpose of the survey.

Conclusion

The magnetometer, which was believed to be the better system for this work, didn't give the expected results. The sidescan sonar output data showed only usable data about the cable shape and position, because structure nearby does not affect sonar survey output results. Since the cable during second survey, has been detected also more to the north, it is likely that it extends over a much longer area. Nature of the semi-buried cable remains unknown.

On this example, it is obvious that several survey methods have to be combined during the semi-buried object detection. Since this survey showed that the large structure presented only interferences on the magnetic data and not the acoustic data, additional survey methods to be involved in this site investigation to get complete information about the semi-buried cable position. This imposes idea of including sub-bottom profile or sub-bottom imager survey method which is completely independent of the large structure influence in surrounding area.

References

De Jong, C.D., Lachapelle, G., Skone, S., Elema, I.A. (2002): Hydrogrphahy, Vereniging vor Studi- en Studetnenbelange te Delft, Delft, 2002.

International Hydrographic Organization: Manual on Hydrography, Publication M-13, 1st edition, May 2005

International Hydrographic Organization: IHO Standards for Hydrographic surveys, Special publication no 44, 5th edition, February 2008

Quintal, R., Dysart, P., Greene, R., "Automated Side-scan Data Analysis," Hydro International, Vol. 11, No. 09, October 2007.

The paper was presented at FIG Working Week 2017, Helsinki, Finland, May 29-June 2, 2017. ▴

Add Performance to your Mobile Mapping Solution



High Accuracy & Cost-effective Inertial Navigation Systems

NEW

Qinertia INS/GNSS Post-processing Software

Geomagnetic Storms: Impact on GPS/GNSS signal delay over the low latitudes

This article demonstrates TEC results at low latitude Indian region, Bangalore (13.020 N, 77.570 E) and Hyderabad (17.410 N, 78.550 E) on the days of high intensity storms (October 29th, 2003), medium intensity storms (March 17th, 2013) and low/no intensity storms (July 05th, 2018)



Dr KCT Swamy
Associate Professor
in ECE at G. Pullaiah
College of Engineering
and Technology, Kurnool,
Andhra Pradesh, India



M A Farida
Assistant Professor in
ECE at G. Pullaiah College
of Engineering and
Technology, Kurnool,
Andhra Pradesh, India



E Upendranath Goud
Assistant Professor in
ECE at G. Pullaiah College
of Engineering and
Technology, Kurnool,
Andhra Pradesh, India

Now a days more than hundred Global Navigation Satellite System (i.e. GPS, GLONASS, Galileo, Beidou, and IRNSS) signals are available everywhere all the time at free of cost. Hence, dependency on the GNSS technology has been increasing with more number of applications in almost all the fields for Position, Navigation and Time (PNT) estimation. The accuracy of GNSS in PNT estimation is being limited by various reasons one among them is dynamic nature of the ionosphere propagation medium which is extended approximately from 60-1000 Km above the earth surface.

One of the reasons for the dynamic nature of the ionosphere is Geomagnetic storms that occur in the interplanetary space. Moreover, an equatorial phenomenon is additional threat to the signals in low latitudes like India. A Geomagnetic Storm is a sudden and temporary disturbance of the Earth's Magnetosphere caused by changes in the solar wind and interplanetary magnetic field (IMF). The disturbance in the interplanetary medium that drives the storms are due to a solar coronal mass ejection (CME) or a high speed stream (co-rotating interaction region or CIR) of the solar wind originating from a region of weak magnetic field on the Sun's surface.

Also, the frequency of storms changes with Sun Spot Number (SSN). Most of the storms that occur during the solar maximum period are CME driven whereas the storms of solar minimum period are

CIR driven. Storms lead to many changes in the plasma, magnetic and electric fields and currents in the Earth's magnetosphere. However, the space weather description and characterisation of geomagnetic storm can be done by measuring the Disturbance Storm time (Dst) index and planetary geomagnetic disturbance index (Kp), Sun Spot Number (SSN), Solar activity, interplanetary magnetic field (IMF) etc. In order to demonstrate and describe impact of the Geomagnetic Storms, three days of different storm intensity levels have been chosen with the Kp index of $4 < Kp < 9$ (29-10-2003), $2 < Kp < 7$ (17-03-2013) $1 < Kp < 5$ (05-07-2018). SSN for the corresponding days is 330, 126 and 0 respectively.

The interplanetary magnetic field direction (Bz) towards the south with values of -10 nT and lower are the indicators for the geomagnetic storm. Figure 1, shows IMF direction (Bz) for different storm days. On October 29th 2003, the geomagnetic storm began to develop at 5:58 UTC when the Bz dropped suddenly from 0 to -35.51 nT and within five minutes it turned to Bz: 5.07 nT at 6:03 UTC. Further it reaches minimum at 6:32 UTC, Bz: -53.85 nT and it reaches positive peak Bz: 34.86 nT at 6:44 UTC. The Bz value remains negative from 18: 11 UTC to 23:59 UTC. Also, the flares occurred on that day are C, M, and X type, among all more intense one is X10.0 flare that happened around 21:00 UTC and a good correlation could be observed between IMF and solar activity. For March 17,

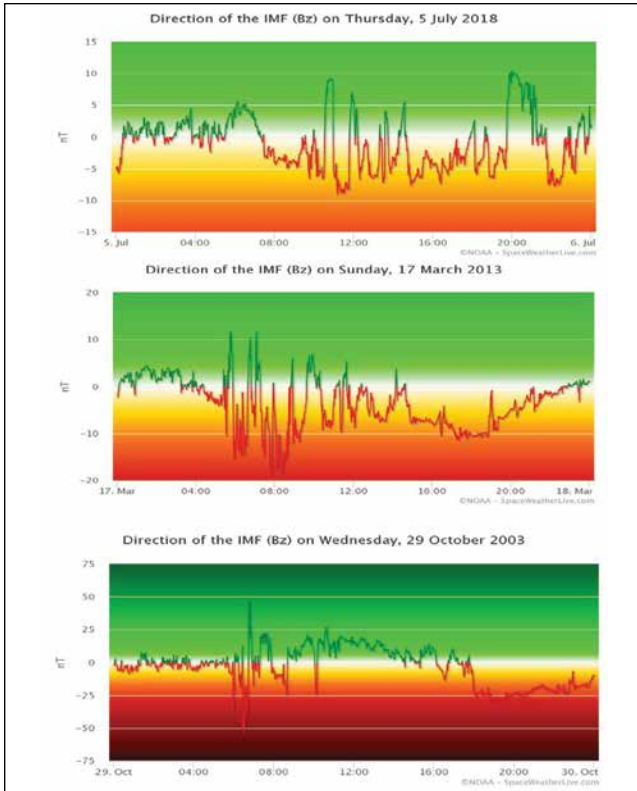


Figure 1: IMF direction (Bz) during various Geomagnetic storm conditions

2013 IMF direction (Bz) is less than -10nT was observed from 6:02 UTC to 9:10 UTC. But on the quiet day (July 5th, 2018) Bz value never reached to -10 nT so as to cause the storm.

One of the major effects of geomagnetic storm on GNSS signal is refraction, due to this signal spends an extra amount of time in the propagation medium and it can be expressed as,

$$\Delta t = \left(\frac{40.3}{cL^2} \right) .TEC$$

(Seconds)

Where, 'c' is velocity of light (i.e. 3x10⁸ m/s), 'L' is carrier signal frequency in Hz. Total Electron Content (TEC) indicates the number of free electrons present along the signal path and is expressed in TECu (1TECu=10¹⁶ electrons/m²). Using dual frequency GPS receiver pseudoranges (P1 and P2), Total Electron Content (TEC) along the signal path can be estimated as,

$$TEC = \frac{1}{40.3} \frac{L_1^2 L_2^2}{(L_1^2 - L_2^2)} (P1 - P2) \quad (TECu)$$

Where, L₁ (1.575 GHz) and L₂ (1.2747 GHz) are the carrier frequencies of GPS.

In this article to analyse the impact of geomagnetic storms on GNSS signal delay, the TEC was estimated for the days of storm (October 29th 2003 and March 17th 2013) and we further compare

<http://www.smartgeoexpo.kr>



SMART GEOSPATIAL EXPO 2018

Geospatial Information for All, Empowering the Future

Sep. 12 - Sep. 14, 2018
COEX, Seoul, Republic of Korea

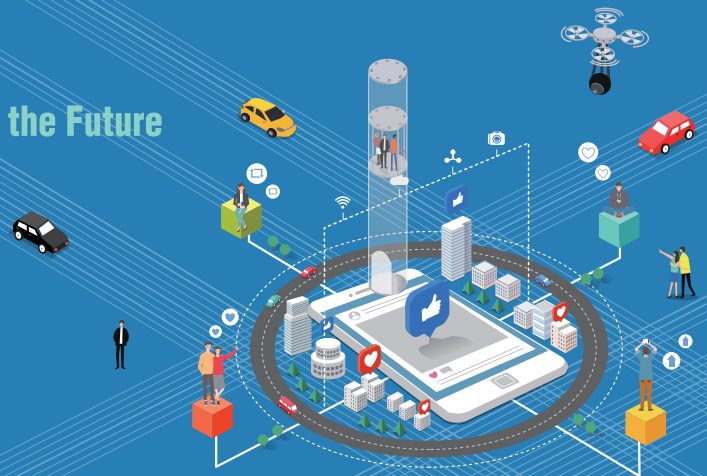


Table 1 Mean and maximum TEC observed during different intensity of Geomagnetic storms

| | 2003-10-29 | | 2013-03-17 | | 2018-07-05 | |
|------|------------|--------|------------|--------|------------|-------|
| | mean | max | Mean | max | Mean | Max |
| HYDE | 71.96 | 330.15 | 54.61 | 220.53 | 12.49 | 84.45 |
| IISC | 68.41 | 293.89 | 54.55 | 197.05 | 11.48 | 46.88 |

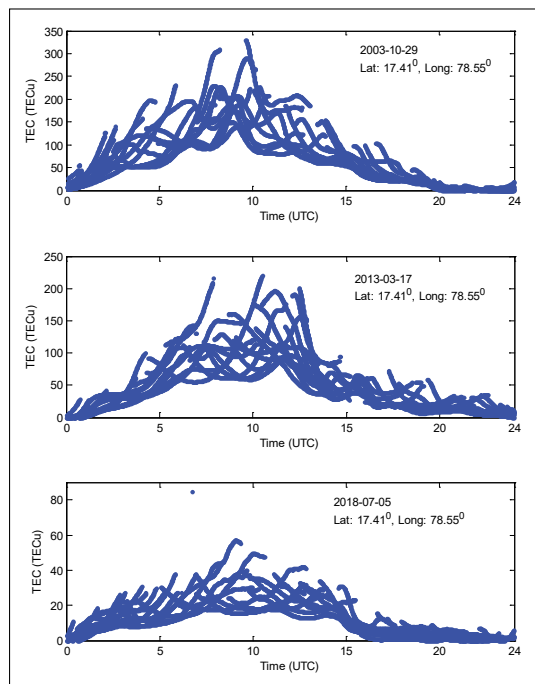


Figure 2. TEC variation on the days of different Geomagnetic intensity levels over the IGS station located at NRGI-Hyderabad

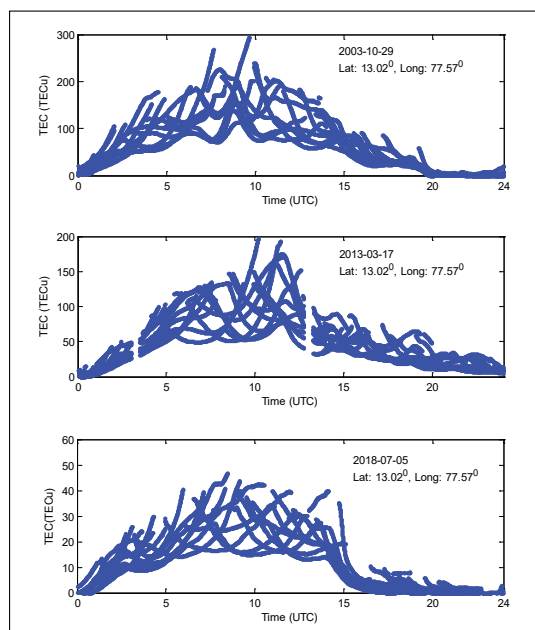


Figure 3. TEC variation on the days of different Geomagnetic intensity levels over the IGS station located at IISC-Bangalore

that of quiet day (July 5th 2018). The required dual frequency GPS receivers data was obtained from IGS network (<http://sopac.ucsd.edu/dataBrowser.shtml>) which was measured on frequencies (L1=1.575 GHz and L2=1.227 GHz) at two low latitude stations (Bangalore (13.02° N, 77.57° E) and Hyderabad (17.41° N, 78.55° E)). GPS data obtained from IGS network is in hatanaka format. By using CRX2RNX tool data was converted into compact RINEX observation file format. For IISc-Bangalore station data is unavailable during 2.99 Hrs-3.50 Hrs and 12.74 Hrs- 13.25 Hrs on 17th March 2013.

Figure 2 and 3 shows the TEC variation of three different geomagnetic activity days at HYDE and IISC IGS stations. At each epoch, selected IGS stations are able to get signals from a minimum of eight satellites. Therefore, TEC is computed for all the available satellite signals and plotted with respect to time. For an instant, consider HYD IGS station on 29th October, 2003, during the mid-day at 10:00 UTC more signals are available and delay measured was not same for all the signals it is varied between 80 TECu and 330.15 TECu. This is because the signals received are at different elevation angles, the low elevation angle signals have long path so it faces more number of free electrons.

TEC introduces a delay of 0.165 meters for the L1 frequency and 0.248 meters for the L2 frequency. As expected, during daytime the TEC increased with time and has reached peak at 10 hrs (UTC) then decreased.

We observe a good correlation between the ionospheric variations and intensity of geomagnetic storms

During geomagnetic storms on (29-10-2003 and 17-03-2013) significant enhancement in TEC is observed compared to the quiet day (05-07-2018), it is upto 390% at Hyderabad station and 260% at Bangalore station (Table 1). This drastic change in ionosphere TEC is due to the changes in the Earth magnetosphere. On storm days Kp-index, SSN, Solar flux are high further the solar flares are also high intense during storm days.

We can notice that during less/no intense storm, TEC maximum does not exceed 60 TECu. During main phase of the geomagnetic storm (29/10/2003) maximum TEC were observed over the selected low latitude stations Hyderabad (330.15 TECu) and Bangalore (293.89 TECu).

On the overall, we observe a good correlation between the ionospheric variations and intensity of geomagnetic storms. Storms induced ionosphere cause significant enhancement in TEC and also rapid changes. Therefore, the consequences of dynamic ionosphere such as time delay and scintillations degrade the performance of GNSS and other satellite based communication systems.

Acknowledgement

The research work presented in this article has been funded by the SAC (ISRO) under the NavIC-GAGAN Utilization Programme, Project ID: NGP-12, Dated: 23 January, 2017. Project title “Investigation of Indian Ionosphere Irregularities Correlation with Space Weather Parameters for Navigation Applications”.

References

<http://sopac.ucsd.edu/dataBrowser.shtml>
<https://www.spaceweatherlive.com> ▢

LIVE at www.javad.com



G'day, Mate!

Redefining Total Stations
and GNSS workflow.

The **“Total Solution”**

From the company who brought you the best GNSS receiver on the planet, our latest innovation will allow you to break away from decades-old methods of measurement and positioning. Why employ a workflow designed for yesterday's gear?

And all
components
fit in this small
carrying case.



*We plan to ship by
September 2018.*

See the video at www.javad.com for proof!

JAVAD



Introducing J-Mate

Why follow a workflow designed for yesterday's equipment?

This is J-Mate

J-Mate features a **camera** that can also find targets automatically, and a **laser module** for accurate distance measurements. It scans and examines the area around the intended target to ensure reliable identification. Two **precision encoders** measure vertical and horizontal angles to the target. Three **precision vials** allow a visual check on levelness of the instrument.



Take control with J-Mate + TRIUMPH-LS

Similar to using conventional total stations, to use the J-Mate you need first to establish its accurate position and calibrate its vertical and horizontal encoders. Then proceed to shoot the unknown points. This is similar to using any total station, but we have improved and automated the process.



Motors

Vials

Laser

- scanning
- distance measurements
- examine area around targets

Camera

- find targets automatically

You can click any point on the screen and the J-Mate will target it by bringing it to the crossbar.

Click the **camera icon** on the top right of the screen to select between the **wide angle of the TRIUMPH-LS camera (60 degrees)** and the **narrow angle of the accurate side camera (5 degrees)**. Select the TRIUMPH-LS camera only for bringing the target close to the center and then switch to the side camera for accurate positioning of the target.

You can also lift the TRIUMPH-LS from the J-Tip and aim it at the direction of the target and the J-Mate will follow. You can also use the J-Tip to point to the target and the J-Mate will follow. Then use the navigation arrows for accurate targeting.



Each click of the navigation arrows move the cross bar according the angle that is selected on the bottom right of the screen (**Navigation Step**). Select the **unit** (Minutes, degrees, or seconds) and the **number**.

The numbers on the top right of the screen show the **linear distance values of the “Navigation Step” and the “Scan Step” at the target point**. It is simply the measured range multiplied by the sine of “Navigation Step” and “Scan Step” angles.

To select the **Snap mode** click the icon above the left arrow. In snap mode the J-Mate moves in the direction of the clicked navigation button until the range is jumped by the **Edge Depth** value.

Use the **zoom buttons** for zooming.

If you want the target to be automatically selected by the **“+” target sign**, click the icon on the top left.

When your target is selected, click the **“Take” icon** on the bottom right of the screen to mea-

sure it according to the **“Target Size”**, **“Scan Step”**, and **“How Many” parameters**. The result of the measurement and the statistics are shown next. Then you can reject or save and assign attributes like a normal RTK point.

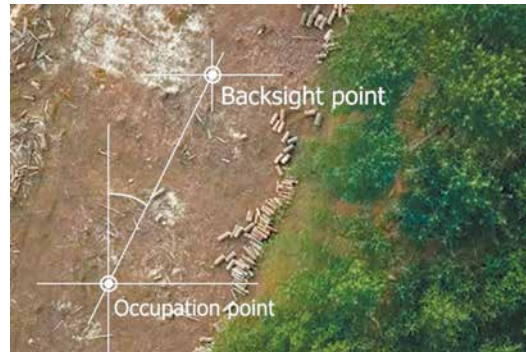
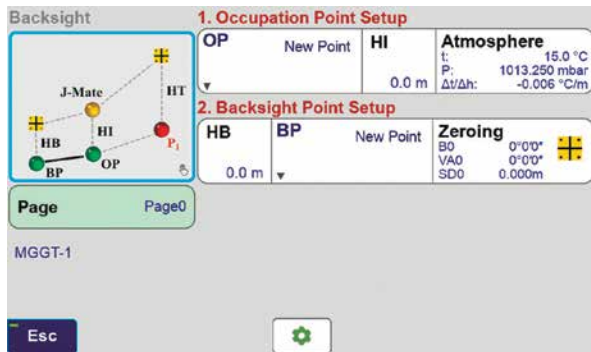
The **“View” icon** shows/hides some icons when you want to focus only on navigation arrows and take measurement.



After the J-Mate is calibrated, you can proceed with your work as normal via the Collect or Stake icon.

Backsight icon

If GNSS signals are available at the job site, click the J-Mate Backsight icon.



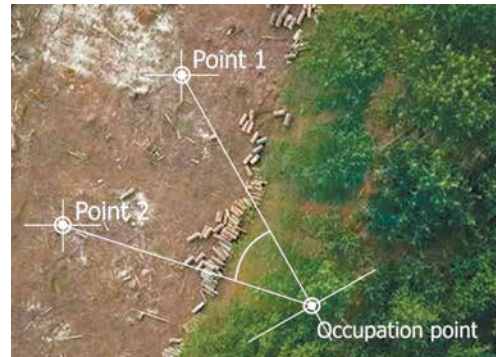
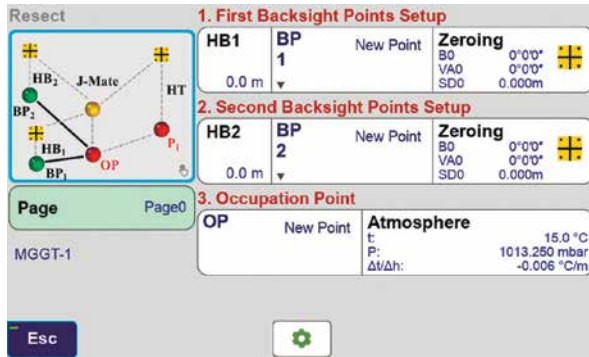
This screen appears which guides you to determine the accurate positions of the Occupation Point and the Backsight Point, to establish an azimuth and calibrate the J-Mate angular encoders.

- The tripod is setup at the “Occupation Point” (OP).
- The J-Mate is secured on the tripod.
- Next, TRIUMPH-LS is placed on top of the J-Mate with its legs registered to the matching features on the J-Mate.
- Next, Use the RTK Survey feature of the TRIUMPH-LS to quickly determine the accurate location of the Occupation Point. You can use your own base station or any public RTN.
- Next, slide the Plus sign target on top of the TRIUMPH-LS, lift it from the J-Mate and move to the “Backsight Point” (BP). The camera of the J-Mate will robotically follow the plus sign target. The camera’s view is visible from the TRIUMPH-LS screen, which mostly focuses on the plus sign. When at the Backsight Point, its accurate position is determined by the TRIUMPH-LS, and the Azimuth from the Occupation Point to the Backsight Point is established, and the J-Mate is calibrated and ready to shoot other points.
- After this calibration is complete, if the tripod is disturbed, the red LED on the front of the J-Mate will blink to show that re-calibration is required.
- We can now replace the TRIUMPH-LS on top of the J-Mate at the Occupation Point and proceed to shoot as many “Target Points” as the job requires. From now on the TRIUMPH-LS is used as a controller and you can hold in your hand too, but it is more convenient to put it on its place on top of the J-Mate to have free hands.



Resect icon

If GNSS signals are not available at the Occupation Point, click the “J-Mate-Resect” icon



Shoot two or more known points to establish an accurate position and calibrate the encoders. Then continue to shoot the unknown points.

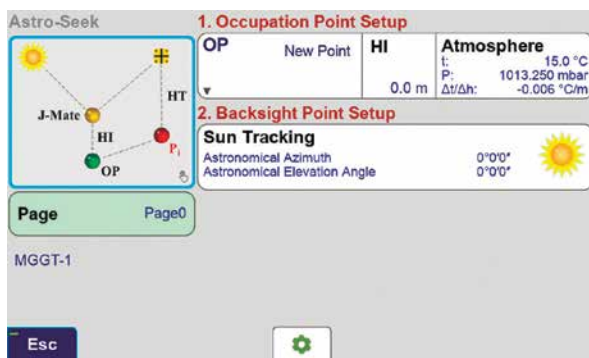


The “J-Mate Resect” automatically finds the plus sign “+” that you carry to two, or more, known points, and shoots them to determine the accurate position of the J-Mate and the azimuth to calibrate the encoders of the J-Mate and then you can proceed to shoot other points.



Astro-Seek icon

And now our new feature!



We have added a new innovative feature

to the J-Mate that it can automatically calibrate itself via its automatic Sun or other astronomical objects-Seeking feature.



If doing a sun-shot, attach the Sun filter to the J-Mate



Then click the “Sun” icon in the screen which appears

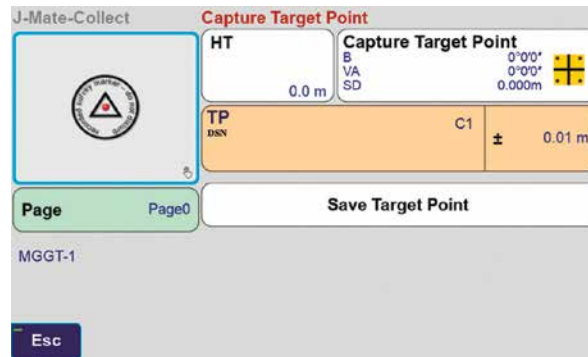


J-Mate will automatically find the Sun, and use its position to calibrate the angular encoders automatically.

Click the “J-Mate-Astro-Seek” icon

J-Mate-Collect

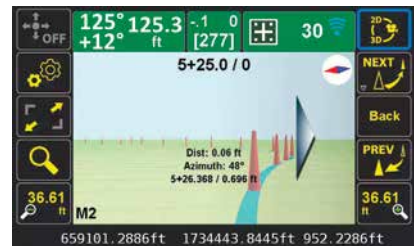
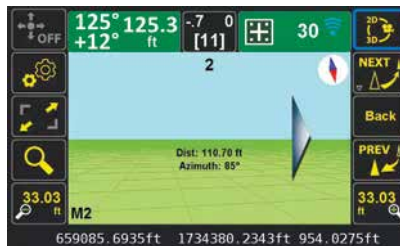
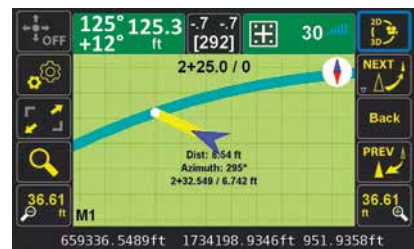
After calibration is performed, click the J-Mate Collect icon to shoot the unknown points.



J-Mate-Stake

Click the J-Mate Stake icon to use the J-Mate for stakeout.

The functions and features of the J-Mate stakeout are very similar to our conventional GNSS stakeout: RTK solutions guide you to the stake points. But with the J-Mate the camera follows the “+” sign that you carry and then the encoders and laser measurements (shown on screenshots) provide guidance to the stakeout features. This is similar to Visual Stakeout and other useful and innovative features of our TRIUMPH-LS GNSS RTK stakeout.

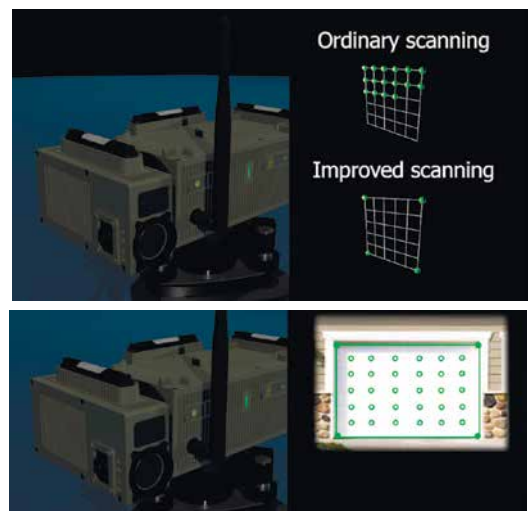


Seize the day with J-Mate + TRIUMPH-LS

Smart laser scanner

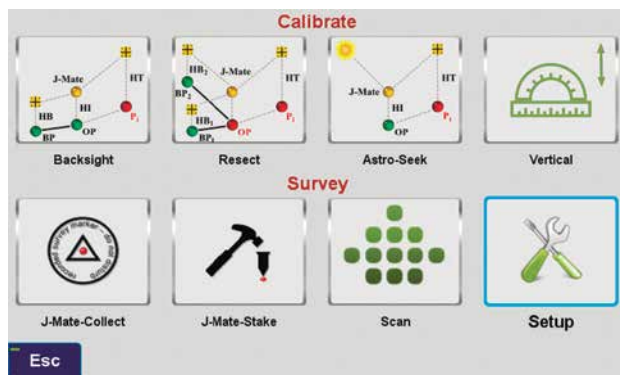
J-Mate is also a camera-aided, smart laser scanner. The camera identifies redundant points that do not need to be scanned, but instead can be copied or interpolated from other readings without loss of information. That is, if the camera identifies a completely uniform flat area, it only scans the four corners of that area and interpolates in between. This feature can increase the effective speed of the scanner to much higher than its native 10-points-per-second speed.

The scanning feature can also be used to find items like wires and poles and “closest-in-view” items and shoot them automatically.



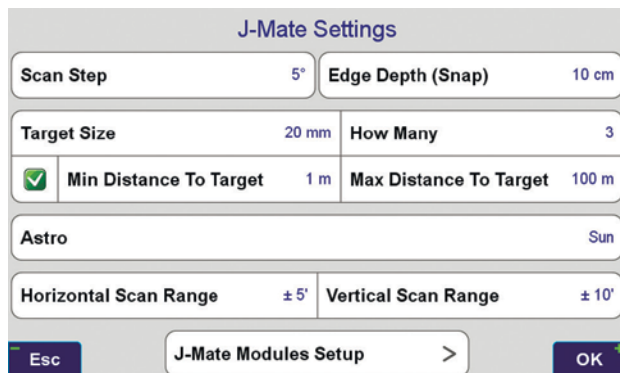
So we have a “**Total GNSS**” with a “**Robotic Total Station**” and a “**Smart Laser Scanner**”. We call it our “**Total Solution**” and it can be operated by one person to perform jobs.

Let us first explain some details of J-Mate operation.



With J-Mate you can establish your occupied position via three different ways: 1) Backsight; 2) Resection; or 3) our new Astro-Seek (more of that later).

When you click the Setup icon of the J-Mate screen you get access to parameters that tunes J-Mate to your desire.



“Scan Step” defines the angular resolution for scanning around the target (according to the target size parameter below). These measurements are examined and averaged to get reliable and more accurate measurement. It is also used as resolution for the scanning operation.

“Edge Depth (snap)” value is used in Snap operation. In Snap mode of the camera screen, the move in the direction of the navigation arrow continues until the range measurement jumps by this value. The snap mode is particularly helpful in automatic identification and measurement of

narrow items like poles.

“Target Size” defines the size of the target that you want to be scanned and averaged with the resolution specified in the the Scan Step.

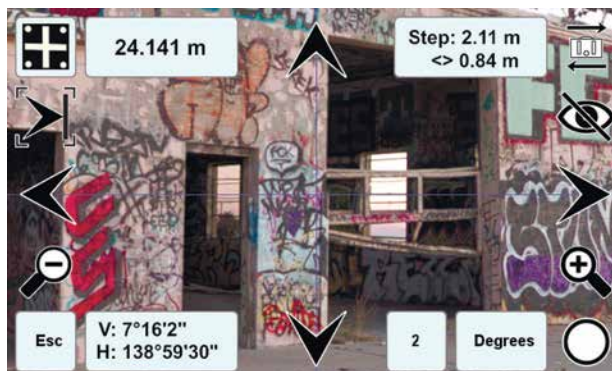
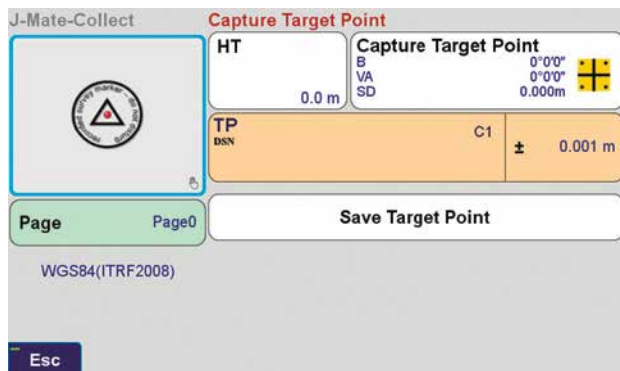
“How Many” defines the number of times you want the target area to be scanned and averaged according to the “Scan Step” and “Target Size”.

The optional Min and Max to Target, when selected, causes the objects outside this range to be ignored and skipped in navigating towards the target and in snap mode.

“Astro” selects the astronomical object to be automatically sought for calibration.

“Horizontal and Vertical Scan Range” defines the angles on both sides of the current center to be scanned in Scanning operation.

When you want to shoot a point click the J-Mate-Collect icon and then click the “Capture Target Point”.

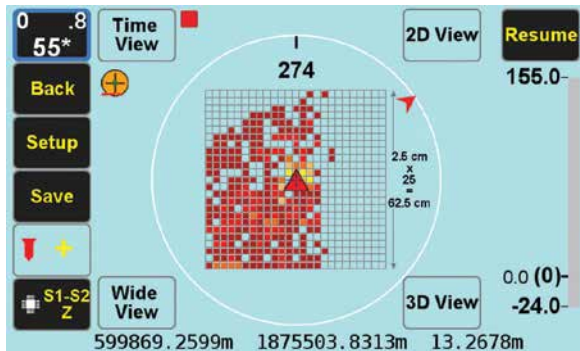


This screen appears which is the camera view of the target. Target is the item that is exactly on the center of the screen on the cross bar.

The range to the target is shown on the box on the top left of the screen and the horizontal and vertical angles on the bottom left.

J-Tip

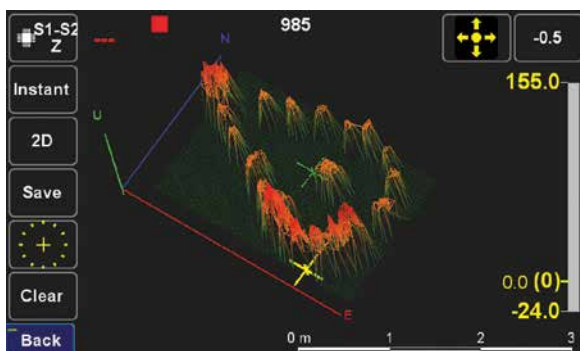
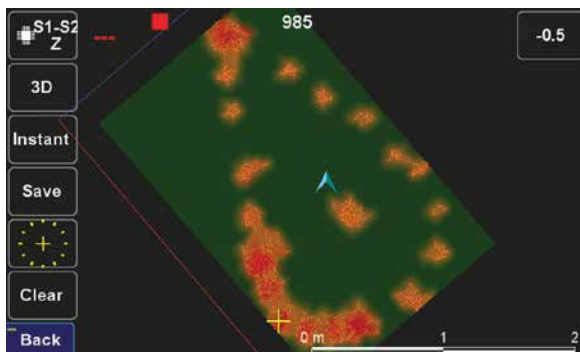
TRIUMPH-LS tags coordinates with magnetic values, It also guides you to top of the item to survey it.



The Mag View focuses only on the mag object with the highest mag value.

The audio and graphical bar on the right side show the magnitude of the magnetic object.

In "Setup" you can select the cell size and the size of the field you want to scan.



The J-Tip has far exceeded my expectations. It is a tool that I have thought about daily my whole career. My thoughts used to be why can't they (whoever they are) make a metal locator that will fit in my pocket. Well, you did it! Yesterday, I was working on a 14 acre boundary survey in steep mountain country. I was able to recover every corner I searched for using the audible tones. I was more effective and efficient than in the past and realized that you have cut the weight and bulk of a metal locator to a fraction of what it was. The J-Tip is lighter than my phone and it fits in my pocket! The locators that I previously used are now collecting dust. They were heavy and cumbersome to tote around. One particular locator that I have used thru the years had a holster and would hang on your side. The back of my knees have taken a beating from that thing slapping the back of them with every step. The J-Tip proved itself to be tough and durable on the mountain survey project. I was also providing topography on a few acres of the site that was covered with green briars, saw briars, kudzu, and very thick. I left the J-Tip on the monopod while working in the brush. Minor scratches are to be expected in that type of environment, so it has a few but the J-Tip took a beating yesterday and worked like a mule. Very impressive!

Adam Plumley, PLS

2D and 3D views of the field show the magnetic objects that have been scanned.

Zooming the 2D and 3D screens can show the shape of the magnetic objects under the ground.

For many sophisticated features of the J-Tip see its Users Manual in www.javad.com

Opportunities and practical use of Android GNSS Raw Measurements

This article presents information on opportunities and practical use of Android GNSS raw measurements. It also presents preliminary results of several testing activities



Justyna Redelkiewicz
European GNSS Agency

In May 2016, Google announced the availability of GNSS raw measurements from Android 7. Since then, the developers can access carrier and code measurements and decoded navigation messages from mass-market devices.

The availability of raw measurements is interesting also from a technological innovation point of view. GNSS raw measurements may support internal smartphone integrity by providing additional sources of information and allowing for the exploitation of receiver autonomous integrity monitoring algorithms.



Martin Sunkevic
European GNSS Agency

There are several advantages of using GNSS raw measurements. Their use can lead to increased GNSS performance, as it opens the door to more advanced GNSS processing techniques that, until now, have been restricted to more professional GNSS receivers. These benefits have been demonstrated through Code Based Positioning, Code Aided Positioning, Differential Positioning and Precise Point Positioning. Although in normal conditions, the position calculated from GNSS raw measurements may not be as optimal as a typical chipset output, in certain cases, when applying external corrections, using GNSS raw data may lead to improved accuracy of the solution. Several application areas stand to profit from this increased accuracy, such as augmented reality, location-based advertising, mobile health and asset management.

This article presents information on opportunities and practical use of GNSS raw measurements. It also presents preliminary results of several testing activities, which showcase working solutions based on GNSS raw measurements and in particular for Galileo. The content is based on “White Paper on using GNSS Raw Measurements on Android Devices” (3) where more details on raw data extraction and its processing are described.



Paolo Crosta
European Space Agency



Moises Navarro-Gallardo
Airbus GmbH



Lukasz Bonenberg
University of Nottingham

The raw measurement also allows to optimise the multi-GNSS solutions, and to select the satellites based on their performances or differentiators. This is particularly relevant for Galileo, which already today offers excellent performances and signal advantages, such as the second frequency E5, and will soon be offering differentiators such as the authentication on the Open Signal E1 and the Precise Point Positioning (PPP).

Android Raw measurements within the GNSS receiver architecture

A GNSS receiver processes signals and provides the user with an estimated Position, Velocity and Time (PVT) solution. This PVT is based on the measured pseudoranges, information delivered through the navigation message, and optional assistance and augmentation provided by third parties. A generic block diagram of a GNSS receiver is shown in Figure 1.

The Radio Frequency (RF) block (the left

side of the diagram) includes the antenna and front-end, which are required for analogue signal processing. It can also include a low noise amplifier, filters and an intermediate-frequency down conversion. The final element in the block is the Analogue-to-Digital Converter (ADC).

In a smartphone, the base-band and PVT processing blocks (right side of the diagram) are software-based signal processing units that are designed to operate on a general-purpose hardware. The baseband processing is responsible for acquiring and tracking of the GNSS signals and decoding the navigation messages. Assisted data (external information) can be provided to reduce the time to fix.

The baseband processing block provides the raw data to the PVT block, which then computes the receiver's PVT. This

process benefits from augmentation data (e.g. EGNOS) or accelerometers (sensors fusion), improving the accuracy and availability in harsh environments.

Android 7 users can use android.location Application Programming Interface (API) to access the raw data required to calculate pseudoranges and decode navigation message (indicated by the red arrow on Figure 1). This data can be used to explore new algorithms and applications for mass-market devices.

The smartphone GNSS/navigation chip acts as a black box and outputs only the PVT and basic information from the tracked satellites (satellite ID and SNR). In high end models, those chipsets use tight integration with cellular, WiFi and Bluetooth to improve the accuracy and availability of the final position. Some

even use motion/orientation sensors for cross aiding. In most cases, if you want to use RAW measurements, it is recommended to feed your algorithm starting position from the chipset PVT, periodically testing your solution against it.

Raw data architecture

Before Android 7.0, only limited GNSS data was accessible through the framework API Location. In this sense, this API acted as a black box, with PVT position provided as it is, without ability to access pseudoranges, phase, navigation message and time information.

The new API (android.location) provides direct access to both the raw GNSS observations and the PVT solution. Figure 2 shows an unassisted receiver architecture and the main differences between new and old API. For clarity, only newly accessible parameters (white boxes) are depicted. Other parameters, such as C/No or satellite position, are omitted. Pseudoranges are not provided by the new API directly, but the parameters needed to generate them are.

The importance of Time/Navigation message and pseudorange generation

While GNSS is best known for its positioning capabilities, it is also one of the most available and reliable sources of precise time. Each GNSS system uses its own time system and usually, receivers provide only one GNSS time.

Internally, the biases between all the GNSS systems must be taken into account. Some systems provide the time differences to GPS time, for example the Galileo/GPS Time Offset (GGTO) provided in the Galileo navigation message. However, the offsets can be also estimated in the navigation solution.

This precise GNSS constellation's time reference is also referenced to Temps Atomique International (TAI) and Coordinated Universal Time (UTC).

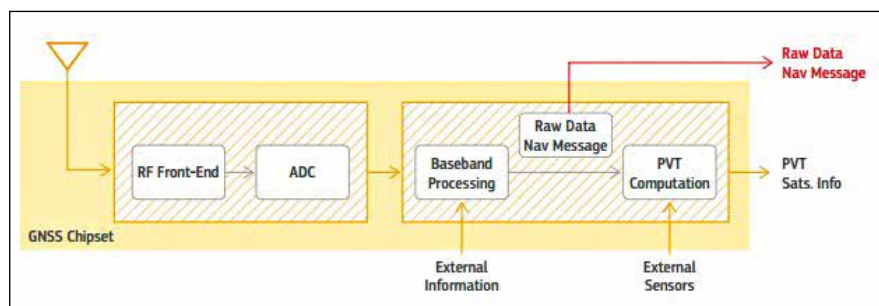


Figure 1 GNSS receiver

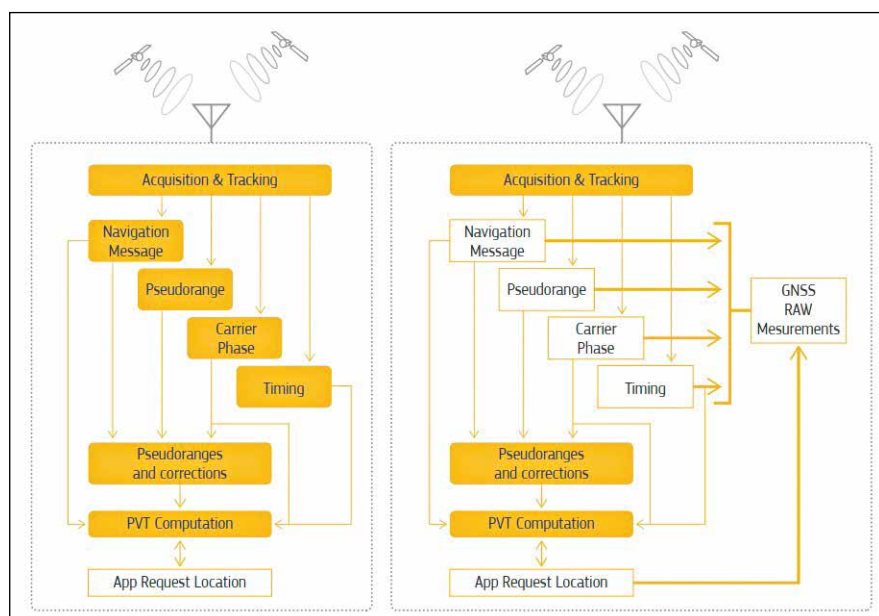


Figure 2: android.gms.location (before Android 7) vs android.location (Android 7)



RIEGL VZ-400i

Ultra High Performance 3D Laser Scanner

Pseudorange generation

Pseudorange is a well-known measurement in the GNSS community, provided as a measurement of distance. However, GNSS receivers derive pseudoranges through time differences. Pseudoranges can be defined as

$$\rho[k] = (t_{Rx}[k] - t_{Tx}[k]) \cdot c$$

where t_{Tx} is the transmitted time, t_{Rx} is the received time, c is the speed of light in vacuum and k indicates the epoch in which the pseudorange is computed (usually known as the measurement time).

The transmitted time (t_{Tx}) can be decoded from the navigation message. Each satellite transmits a time stamp (e.g. Time of Week for GPS and Galileo) at specific rate. Before it is decoded, the transmitted time is ambiguous. The ambiguity depends on the stage of the navigation message decoding process (e.g. primary code or page synchronization).

When unassisted GNSS receivers are initialized, GNSS time information is not available and internal hardware clock (t_{clock}) runs independently. Therefore, the bias between the internal clock and the GNSS time must be roughly estimated in order to compute the received time.

This is done by assuming that the initial received time ($t_{clock}[1]$) is the transmitted time of the first satellite ($t_{Tx,sat1}[1]$) plus the reference propagation time (t_{ref}^{path}). Typical values are between 65 and 85 ms. hence, the bias can be expressed as

$$b = t_{Tx,sat1}[1] + t_{ref}^{path} - t_{clock}[1]$$

and the received time can be expressed as

$$t_{Rx}[k] = t_{clock} + b$$

Therefore, pseudoranges can be generated as

$$\rho[k] = (t_{clock}[k] - t_{Tx}[k] + b) \cdot c$$

In (3) a similar approach using the first clock bias estimation instead of the reference propagation time is shown.

Since the bias has been roughly estimated, the residual error is introduced in the clock



Proven in the Field:

Extremely Fast Data Acquisition,
Automatic On-Board Registration, User Friendly!



- » **NEW** Automatic registration during data acquisition – **Tremendous time savings!**
- » Up to 1.2 million measurements/sec – **Extremely fast data acquisition!**
- » RIEGL Waveform-LiDAR technology – **Highly informative and precise data!**
- » Cloud connectivity via LAN, Wi-Fi and LTE 4G/3G – **Worldwide access for smart remote scanner control and data upload!**
- » Customizable workflows – **High field efficiency!**
- » User-friendly touch screen – **Easy to operate!**





RIEGL VZ-1 On-board
Registration Video on
our YouTube Channel
online!

www.riegl.com



bias of the PVT solution. The deviation due to the clock precision is also absorbed in the PVT. It should be noted that when multi-constellation PVT solution is computed, the biases between the constellations must be taken into account.

Opportunities and practical use of GNSS Raw Measurements

The architecture of GNSS mobile chipsets prioritises the user experience by minimizing TTFF (time to first fix) to seconds and by improving position availability and continuity. Recently enabled raw measurements, available via android.location API, allow us to use the advanced positioning techniques summarised in Figure 3, which reduce GNSS error and can improve positioning accuracy. Raw measurements also support integration with the other sensors found inside the mobile phone and, with additional observables (such as Doppler and SNR), can provide better accuracy estimation, navigation robustness and an additional layer of security.

Mobile A-GNSS Chipsets overview

Mobile phone designs focus on battery optimisation and user experience, which impact both the selection of hardware components and software algorithms. Two different kind of oscillators are typically used in mobile phones: the TCXO that compensates the temperature variations and a low-power computation crystal oscillator (OX) that maintains the time with an accuracy degradation of 6 seconds per week (5).

A-GNSS chipsets are designed to reduce the TTFF within a few seconds using built-in access to the communication device (such as a 4G modem or WiFi connection) in order to retrieve time satellite information.

The mobile device will improve the reference frequency by calibrating the local oscillator in the phone (5)

and it will obtain the approximate estimation of the smartphone position and the assistance data (5) (6) (7).

The typical antenna used in mobile phones is an inexpensive, PIFA (Planar Inverted-F Antenna). Its linear polarization (instead of circular) and the directivity

of the radiation pattern leads to several dBs of signal loss. The relative loss, with respect to a standard patch antenna, is estimated to be around 11dB with highly irregular gain pattern (8) (9).

Hardware design choices impact the quality of the GNSS raw data, especially carrier

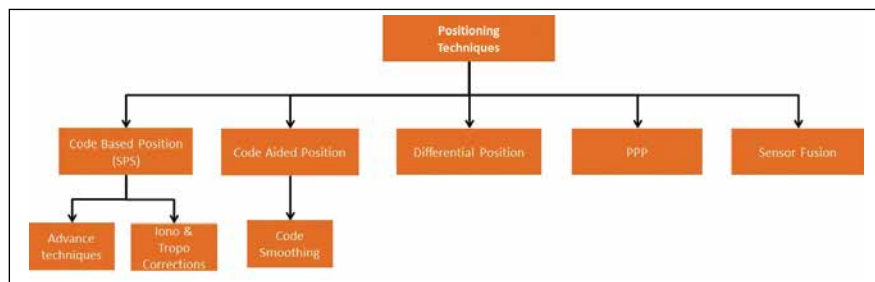


Figure 3 Positioning techniques

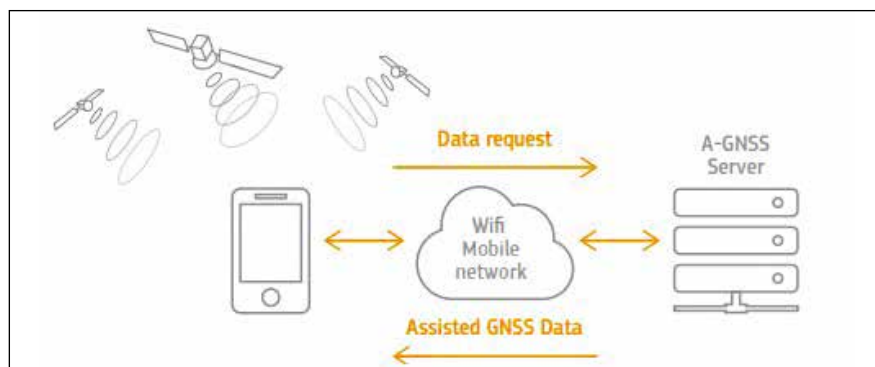


Figure 4 Assisted GNSS

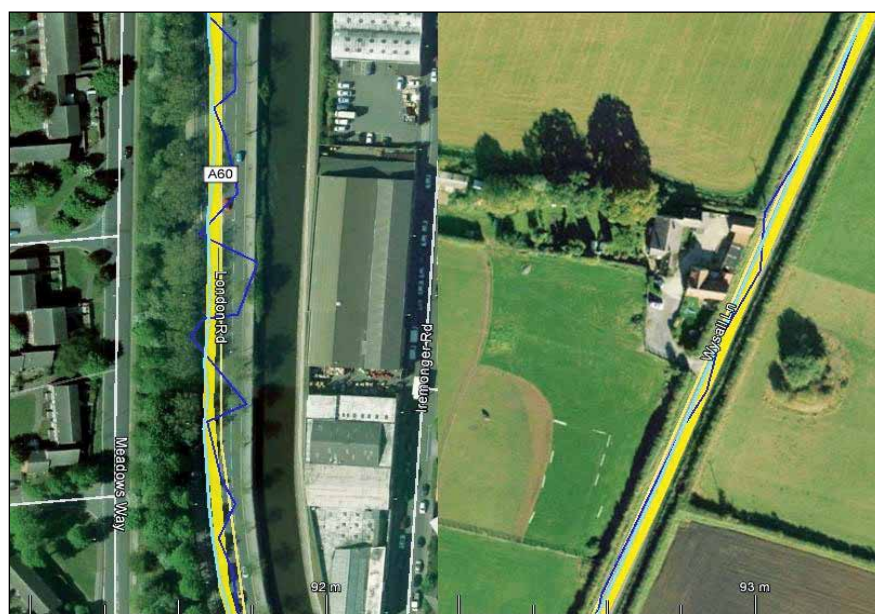


Figure 5: Kinematic test results (results computed and provided by the University of Nottingham)

phase measurements, thus directly affecting the performance of the positioning. Due to increased levels of multipath and a higher probability of fading, this effect will be even worse in the urban environment, where most phones are used.

Baseline performance – Code positioning

Several tests have been conducted in order to assess the performances of Android smartphones using raw data.

First, a dynamic scenario has been considered. The main characteristics of this test are:

- The receiver is placed on the dashboard of a moving car.
- A Nexus 9 tablet has been used, with GPS and GLONASS constellations used.

The results of kinematic trials are shown in Figure 5, where:

- The thick yellow line is the truth provided by the tactical grade Inertial Measurement Unit (IMU).
- The blue line represents the Android solution obtained from the Nexus 9 tablet.
- The green line is a code-only solution obtained using a low-cost single-frequency receiver with multipath-resistant geodetic antenna.

The main contributor to the difference between blue and green lines is mainly the linearly polarised antenna, which is poor at removing multipath in the urban environment (left side image). In the clear rural environment (right side), Android can maintain comparable performance with a low-cost GNSS receiver if no multipath is present and it is being visibly affected by the stray signals from the building on the left.

Improving Position

Multiple constellations

Figure 6 compares 3D instantaneous position error of the PVT solution

calculated first using GPS only (black dots) with the PVT from using three constellations (GPS, GLONASS, Galileo). For simplicity, accuracy increase (error decrease) is visualized by a green dot and accuracy decrease by a red one. While the minimum satellite requirement is four, to obtain a reliable positioning, especially in the presence of noise and obstruction, 8-10 satellites are needed.

In case of limited sky visibility, common in urban areas, this can only be achieved using a multi-GNSS solution. This is visualised by the green circles that cover the top part of the graph - the area of poor GPS performance. In open sky conditions, when 8-10 satellites can be obtained from a single constellation, just increasing their number will not lead to better accuracy. This is mostly due to the build-up of noise and multipath effect, as demonstrated by the cluster of red circles at the bottom of the graph.

In this case, pre-selection of the best satellites for PVT would be recommended over increasing the overall number

above 10. It should also be noted that the Inter-System Biases (ISB) between the systems needs to be properly estimated.

Table 1 quantifies the accuracy and availability of the position for all the constellation combinations, demonstrating the benefit of using multi-GNSS. All data was processed in the open source RTKLib software (1), using kinematic data collected on Android device.

Using information inside chipsets – Doppler smoothing of the code observables

To improve static positioning accuracy, the Hatch Filter to smooth code observation can be used (2). Traditionally, we use carrier phase, but duty cycle introduces repeatable cycle slips that require filter reset. Instead, we can use Doppler measurements that are more resistant to a duty cycle. Figure 7 shows a comparison of a static PVT obtained from raw measurement data using code only and Doppler smoothing, with

Table 1: Multi-constellation impact in PVT accuracy and availability (results computed and provided by ESA)

| PVT Configuration | Horizontal confidence level (meters) | | |
|-----------------------|--------------------------------------|-------|--------------|
| | 68% | 95% | Availability |
| GPS | 13.36 | 25.51 | 97.79% |
| GPS + GAL | 12.48 | 23.78 | 98.04% |
| GPS + GLO + GAL | 11.24 | 21.57 | 98.30% |
| GPS + GLO + GAL + BEI | 11.17 | 21.44 | 98.30% |

Table 2: PVT Kinematic performance comparison – Doppler smoothing (results computed and provided by ESA)

| Multi-GNSS configurations 68% | | Horizontal confidence level (meters) | | |
|-------------------------------|---------------------------|--------------------------------------|--------------|--------|
| | | 95% | Availability | |
| Doppler Smoothing 20sec | PVT GPS | 9.38 | 18.87 | 97.79% |
| | PVT GPS + GAL | 9.21 | 18.63 | 98.04% |
| | PVT GPS + GLO + GAL | 7.72 | 16.65 | 98.30% |
| | PVT GPS + GLO + GAL + BEI | 7.69 | 16.53 | 98.30% |
| No Doppler Smoothing | PVT GPS | 13.36 | 25.51 | 97.79% |
| | PVT GPS + GAL | 12.48 | 23.78 | 98.04% |
| | PVT GPS + GLO + GAL | 11.24 | 21.57 | 98.30% |
| | PVT GPS + GLO + GAL + BEI | 11.17 | 21.44 | 98.30% |

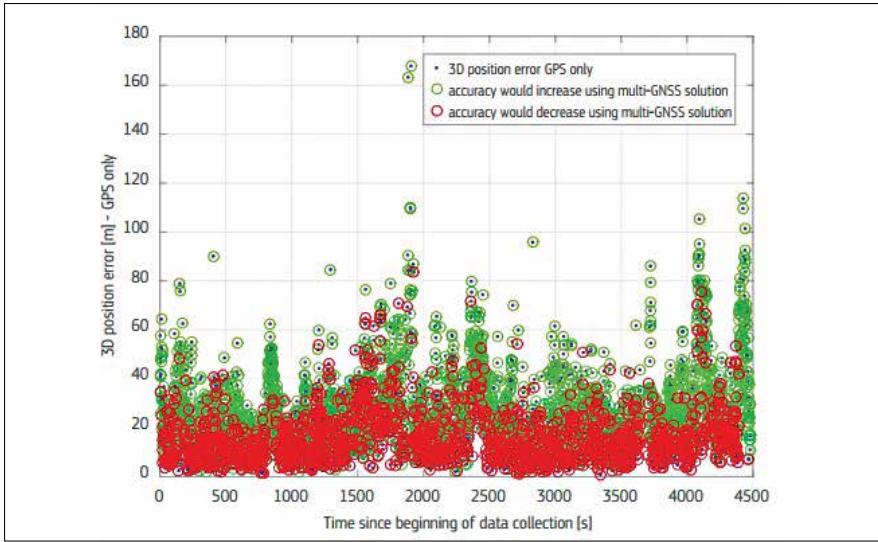


Figure 6: Position error with GPS only and GPS + GAL + GLO (results computed and provided by ESA)

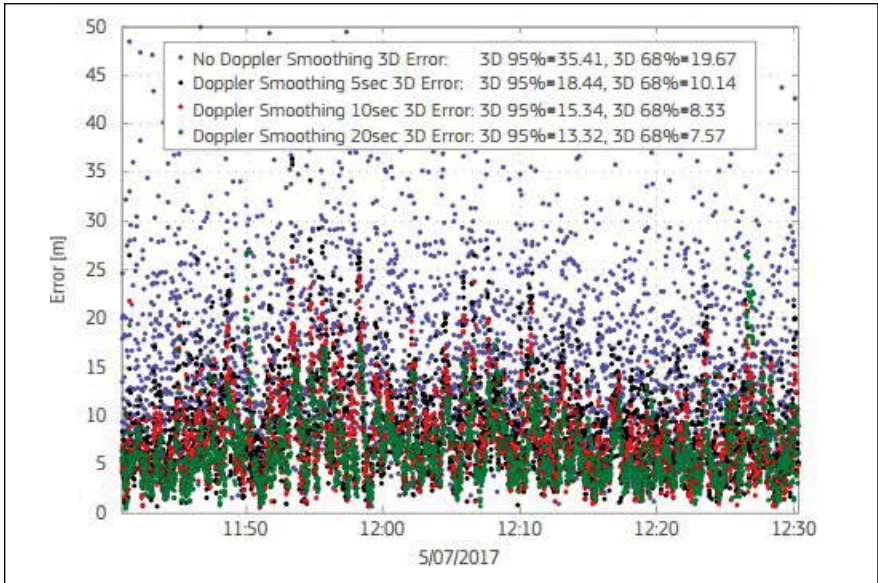


Figure 7: GPS + GLO + GAL PVT performance comparison – Doppler smoothing (results computed and provided by ESA)



Figure 8: PVT Kinematic solutions – Raw code (left) – Doppler smoothed (right)

different integration times. By using a smoothing window of 20 seconds, the 3D error (at 68% confidence level) is reduced by almost a factor of three, from 19.7 metres to 7.6 metres.

To assess this method in the kinematic scenario, let's once again consider the motorway scenario with the 20 seconds smoothing window, which was selected based on the good results achieved with the static scenario. Smoothing increased accuracy, albeit smaller than in the static scenario, leading to a much smoother path, even in the highly dynamic motorway scenario (Figure 8). The reference trajectory (green) has been calculated with a high-end GNSS receiver.

Taking it beyond the phone – differential observations

Primary GNSS error sources are satellite-based (orbits and clock), atmosphere (ionospheric and tropospheric delays), noise and local effects (including multipath). Differential observation improves positioning accuracy by providing external corrections to those errors, but usually does not correct local effects such as multipath or interference. There are several techniques for doing so, with the most commonly used being DGNSS (or DGPS, Differential GNSS/GPS) for code solution and the Real Time Kinematics (RTK), Network RTK and Precise Point Positioning (PPP) for the carrier phase solutions.

The most accurate results can be obtained when using carrier phase in RTK and PPP. Both require a good quality carrier phase and, ideally, a static convergence time to solve the ambiguities and increase the accuracy. Convergence time is considerably longer with PPP, but its data requirement is more flexible. Corrections are transmitted via radio or the internet, but do not provide integrity information. Instead, this is provided by the large area SBAS services such as EGNOS, which also provide a Klobuchar-like ionospheric correction model tailored for Europe and Africa.

This model can be improved by a more localised model like, for example, the bespoke ionospheric correction model for Northern Adriatic for quiet space

weather conditions in the summer time (10). Table 3 and Figure 9 show the difference between processing the static raw observables using a PPP algorithm

(blue) and a device based code-based positioning solution (red). Reference location is indicated by a black cross.

Table 3: Impact of PPP in user accuracy, values in [m] (results have been computed and provided by ESA)

| PPP vs PVT configurations | Static Scenario | | | | |
|---------------------------|-----------------|-------|-------|-------|--------------|
| | H68% | H95% | V68% | V95% | Availability |
| PVT GPS + GAL | 9.18 | 15.43 | 17.43 | 34.67 | 99.70% |
| PPP GPS + GAL | 0.90 | 2.35 | 0.62 | 1.43 | 99.70% |

Table 4 Phase validity (No duty-cycle) per satellite (results computed and provided by Airbus Defence and Space GmbH)

| Satellite | Phase Valid [%] | Cycle Slip [%] |
|----------------|-----------------|----------------|
| Sat 5 | 26.73 | 73.26 |
| Sat 10 | 78.75 | 21.24 |
| Sat 16 | 92.96 | 7.03 |
| Sat 18 | 94.92 | 5.07 |
| Sat 20 | 99.63 | 0.36 |
| Sat 21 | 13.95 | 86.04 |
| Sat 26 | 98.98 | 1.01 |
| Sat 27 | 7.69 | 92.30 |
| Sat 29 | 96.51 | 3.48 |
| Sat 31 | 99.63 | 0.36 |
| GPS Aggregated | 92.86 | 7.13 |

Table 5 Phase validity per satellite (results computed and provided by Airbus Defence and Space GmbH)

| Satellite | Phase Valid [%] | Cycle Slip [%] |
|----------------|-----------------|----------------|
| Sat 1 | 64.05 | 35.94 |
| Sat 3 | 85.29 | 14.70 |
| Sat 6 | 49.72 | 50.27 |
| Sat 9 | 58.81 | 41.18 |
| Sat 11 | 32.45 | 67.54 |
| Sat 17 | 44.26 | 55.73 |
| Sat 19 | 51.76 | 48.23 |
| Sat 22 | 76.47 | 23.52 |
| Sat 33 | 85.34 | 14.76 |
| Sat 31 | 46.23 | 53.76 |
| GPS Aggregated | 59.44 | 40.55 |

This performance can be improved by dual frequency chipsets, which just recently became available for the mobile platform. They provide both L1/E1 and GPS L5 and Galileo E5 signals that are much more resistant to multipath. Initial trials show improved performance and the cycle slip detection and correction (11).

Duty cycle

The duty cycle, deployed by the phone to reduce power consumption, affects the oscillator and introduces the carrier phase tracking discontinuity. Figure 10 shows the static data, collected without the active cycle (function was turned off). More than 90% of the phase measurement is valid, allowing for the use of an RTK or PPP algorithm. Three satellites (5, 21, 27) show an unusually high number of cycle slips, which could be due to a combination of low elevation and noise. These have been removed from the calculations.

The results shows that disabling duty cycle would improve the performance and, as such, is recommended for high precision applications, even at the cost of increased power consumption.

Educational and scientific applications

Raw measurements are also very exciting from a scientific perspective. Android devices can be deployed as a grid of sensors, given the reasonably low hardware cost and no need for dedicated firmware development.

One of the scientific uses of GNSS raw measurements is the provision of detailed atmosphere monitoring using only one frequency. Other applications and uses includes base station deployment, interference detection and as a part of a smart city's sensors.

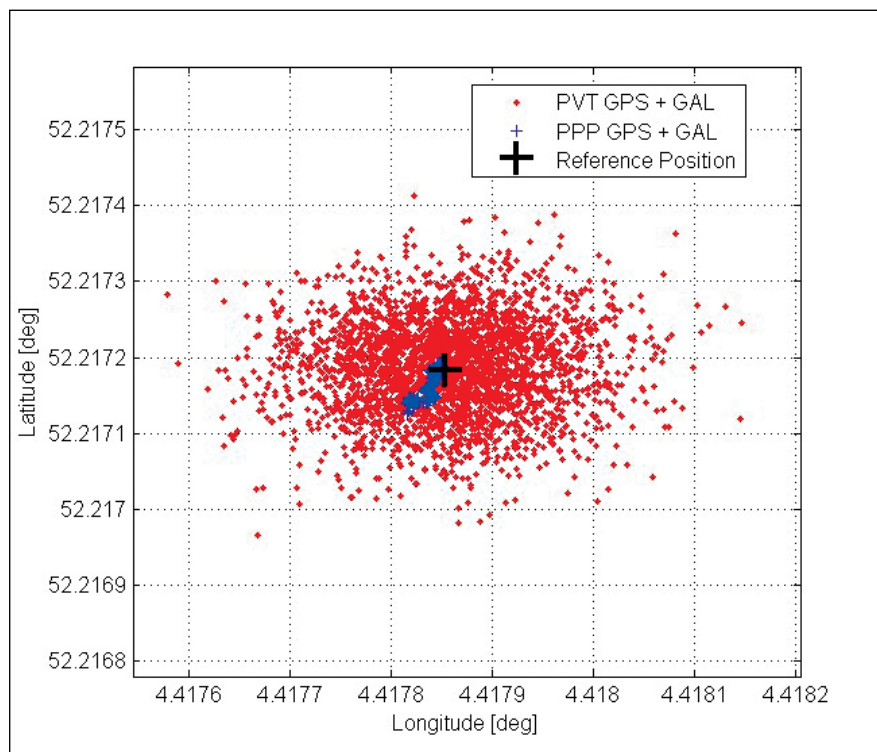


Figure 9 PPP vs PVT Solutions

Secondly, android devices are an excellent teaching tool, allowing one to understand how GNSS measurements are obtained and calculated. Observations can also be used to compare solutions from single constellations (e.g. Galileo-only positioning in Figure 12), eliminate specific satellites or visualise worst-

scenario performance. Apart from education, the same approach can also be used to test hardware and software solutions, observe performance level and compare this performance with the benchmark solution provided by the chipset itself. An example of this is the GNSS Analysis tool provided by Google (12).

High Integrity Solutions

Access to raw measurements, in the form of individual pseudoranges and C/No, as well as Automatic Gain Control (AGC) values, will offer the opportunity to generate new ways to detect RF interferences using the device itself. Furthermore, through the combination of measurement data from multiple Android devices within a region, there will also be the potential to locate the source of the interference. Currently, this may be a niche application, yet access to such capabilities will create opportunities to develop novel services to assist GNSS users, service providers, infrastructure operators and national frequency authorities in protecting the GNSS spectrum.

Receiver Autonomous Integrity Monitoring (RAIM) is an algorithmic assessment of GNSS signal integrity, providing confidence level assessment of navigation performance that can warn a user if performance is below the set threshold and another solution is required. These are intended for the safety-critical GNSS applications, but it can be extended to the Android platform, providing users with better positional confidence, additional verification and warning.

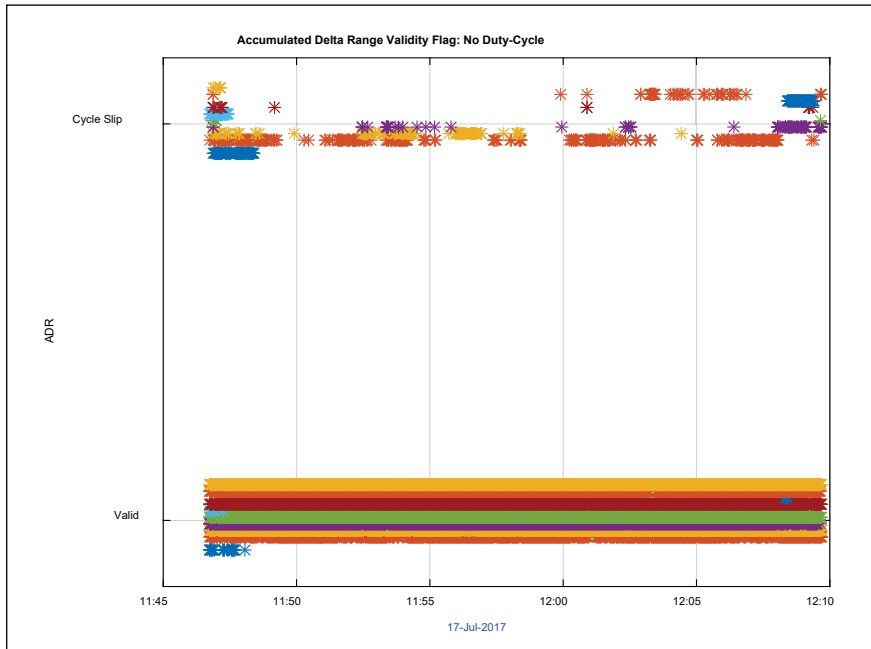


Figure 10 Phase validity (no Duty-cycle) versus time (results computed and provided by Airbus Defence and Space GmbH)

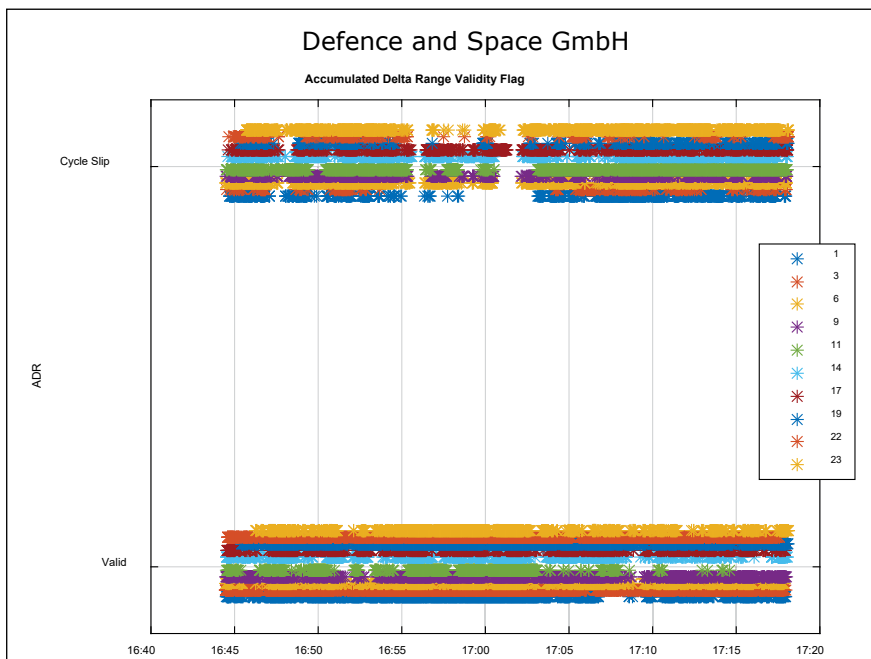


Figure 11 Phase validity versus time (results computed and provided by Airbus Defence and Space GmbH)

The need for higher accuracy in the mass market

Currently, over 6 billion GNSS devices are in use around the world, vast majority of which are smartphones. More than 50% of applications in the Google Play and Apple stores use location information. Smartphones are increasingly used in applications that are at the border of safety-critical or high precision ones, from navigating a glade or leisure boat to mapping trees for city park management. The higher location accuracy that can be obtained in the mass market will further increase the use of smartphones and wearables in semi-professional applications and enable a new range of consumer applications that are still not possible today.

The typical performance of today's mass market mobile devices is in the

range of metres to even tens of metres in difficult conditions, such as urban canyons. However, the use of multi-constellation, dual-frequency chipsets and the provision of external information promise to increase this accuracy to sub-metre levels in the near future.

Android raw measurements will provide additional layers of integrity and robust position, enabling the development of robust, reliable and interference-resilient position-based services.

Existing applications and devices providing the raw measurements

A couple of Android applications are already utilising GNSS raw measurements. The main purpose of these applications is either to convert Android measurements in standardized formats to be eventually used (RTCM, RINEX...) or to allow the user to calculate higher accuracy position by receiving and using augmentation data. Some of these applications are PPP Wizlite, RTCM Converter, Geo++ Rinex Logger, Airbus GNSS Data Collector, Android GNSS Logger, G-RitZ Logger, GNSS Data Recorder, rinex ON.

A list of devices capable of providing raw measurements is maintained at (4).

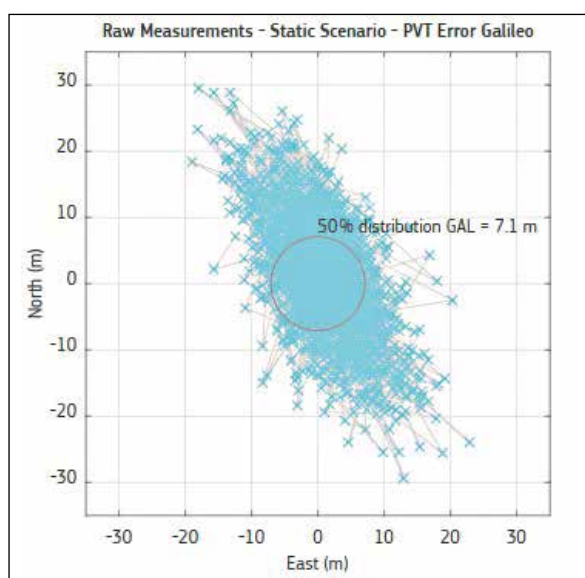


Figure 12 Static Galileo-only positioning error (results computed and provided by Airbus Defence and Space GmbH)

Information also includes constellations availability and the availability of the phase measurements. All devices need to run Android 7 or later.

GNSS raw measurements task force

Soon after the Google's announcement, the European GNSS Agency (GSA) has launched the GNSS Raw Measurements Task Force to engage with leading experts in navigation and positioning, and boost innovation around this new feature (<https://www.gsa.europa.eu/gnss-raw-measurements-task-force>).

The Task Force aims to share knowledge and expertise on GNSS raw measurements and its use, including its potential for high accuracy positioning techniques. The Task Force includes GNSS experts, scientists and GNSS market players from around the world.

GSA is also directly supporting the mobile developers to put the theory into practise. Still this year, GSA is organizing a special tutorial on raw measurements during the Indoor Positioning and Indoor Navigation (IPIN) conference in Nantes in September as well as the "Space for your App" hackathon, taking place in Padua in October. In the first quarter of 2019, GSA in cooperation with GNSS. asia project is planning to organize two regional hackathons in India, exact dates are still to be confirmed. All upcoming events are announced at GSA website: www.gsa.europa.eu.

References

[1] <http://www.rtklib.com/>
 [2] http://www.navidia.net/index.php/Carrier-smoothing_of_code_pseudoranges

[3] European GNSS Agency (2017), White Paper on using GNSS Raw Measurements on Android Devices (https://www.gsa.europa.eu/system/files/reports/gnss_raw_measurement_web_0.pdf)
 [4] <https://developer.android.com/guide/topics/sensors/gnss.html>
 [5] Van Diggelen, Frank Stephen Tromp. 2009. A-GPS: assisted GPS, GNSS, and SBAS. Boston: Artech House
 [6] Nicolas Couronneau (2013) Performance analysis of assisted-GNSS receivers, PhD, University of Cambridge
 [7] <http://rxnetworks.com/location-io/predicted--gnss-ephemeris/>
 [8] Pesyna, K. M.; Heath, R. W. & Humphreys, T. E. Centimeter Positioning with a Smartphone-Quality GNSS Antenna Proceedings of the 2014 ION GNSS Conference, 2014
 [9] Humphreys, T. E.; Murrian, M.; van Diggelen, F.; Podshivalov, S. & Kenneth M. Pesyna, J. On the Feasibility of cm-Accurate Positioning via a Smartphone's Antenna and GNSS Chip Proceedings of the 2016 IEEE/ION PLANS Conference, 2016
 [10] Brcic, D. (2015). A model of non-specific daily pattern of the satellite positioning signal ionospheric delay (PhD thesis). Faculty of Maritime Studies, University of Rijeka. Rijeka, Croatia.
 [11] Riley, S.; Lentz, W. & Clare, A. (2017) On the Path to Precision - Observations with Android GNSS Observable of the 2017 ION GNSS Conference
 [12] GPS Measurement Tools, google. Available at: <https://github.com/google/gps-measurement-tools>

"Mobile mapping has become one of the most important geospatial technologies"

says Stuart Woods, Vice President, Geospatial Content Solutions Division, Leica Geosystems AG.

How is Leica Pegasus: Two Ultimate different from its earlier version Leica Pegasus: Two?

The Leica Pegasus:Two Ultimate is an upgrade to the Pegasus:Two, Leica Geosystem's trusted mobile mapping platform. With a focus on imagery, it removes the need for multiple-camera stitching by incorporating a single stitchless 24 MP 360-degree camera calibrated to the LiDAR profiler for measurements directly from the 360-degree image, enabling true survey-grade digital reality captures from car, train, or boat.

The new Leica Pegasus:Two Ultimate increase the typical working day - allowing capture in a variety of lighting conditions and vehicle speeds - a higher dynamic range is enabled by a large sensor to pixel ratio and a dual-light sensor. Photogrammetry and HD image quality is improved with the increased side camera resolution to twelve mega pixels with onboard JPEG compression.

To enable faster processing at the office, a removable SSD allows to simply eject your data and walk into the office.

What are the key applications for which Pegasus: Two Ultimate is most suitable for?

Digitisation of city and transportation infrastructures, planning, and assets is the foundation of the Smart City, the Leica Pegasus:Two Ultimate enables your growth and ability to offer the best solution for this market. Seamless 360° imagery calibrated to the digital point cloud will help you to deliver easily realised data assets for a future with autonomous vehicles, smart rail, and smart cities.

How cost efficient are mobile mapping systems?

Leica Geosystems' Mobile Mapping Systems increase, in general, the survey productivity up to 20 times. Where environments would have taken weeks to survey, they now only take days, improving efficiency and productivity – while eliminating traffic manage and putting workers at risk.

What has been the growth and penetration of 3D mapping systems in different geographies of the world?

In recent years, mobile mapping has become one of the most important geospatial technologies available and it continues to change the way environments are measured, visualised, analysed, and catalogued. Through Leica Geosystems' world-wide sales and support channels, we have touch every geographical location in the world. There are few countries where a Leica Geosystems' mobile mapping system is not available for demo or a partnership with an existing user. The geographic width of where the Leica Geosystems' technology is power to the strength the technology.

How according to you has mobile mapping technology evolved over the years?

Mobile mapping is now more quick, accurate, and more comprehensive than ever before, and is delivering significant benefits to users and asset owners. Inaccessible areas can be mapped effectively and quickly using the Leica Geosystems Mobile Platforms – through such technologies as SLAM – we are mapping the unreachable. From mapping water pipes to sewer drains to caves, mobile mapping has extended to areas that could never be reached before as they were in GNSS denied areas. Today, by marrying multiple positioning technologies, Leica Geosystems' is able to offer survey-grade accuracy which is accepted as a standard.

Airbus wins two ESA studies for Mars Sample Return mission

Airbus has won two studies from the European Space Agency (ESA) to design a Sample Fetch Rover and an Earth Return Orbiter. These two elements will be critical parts of a mission to return samples of the planet Mars to Earth before the end of the next decade. NASA and ESA signed a letter of intent in April 2018 to pursue a Mars Sample Return mission.

After launching to Mars in 2026, the Mars Sample Fetch Rover will retrieve Mars samples left by the Mars2020 rover. This NASA rover will leave 36 pen sized sample tubes on the Martian surface ready to be collected later.

The Sample Fetch Rover will pick up the sample tubes, carry them back and load them into a sample container within the waiting Mars Ascent Vehicle. The Mars Ascent Vehicle will then launch from the surface and put the sample container into orbit about Mars.

EagleView sets new standard for aerial image capture

Eagle View Technologies, Inc. has announced its intention to acquire Spookfish Limited an Australian listed public company focused on the development and commercialization of premium next generation geospatial imagery products and services. With this acquisition, it simultaneously secures advanced Spookfish aerial camera technology for mass adoption in North America and establishes a presence in the Australian market. www.eagleview.com

NASA launches Remote Sensing Toolkit

To help commercial users more easily take advantage of NASA's remote sensing data, the space agency created the Remote Sensing Toolkit, a website that lets users unfamiliar with aircraft and satellite data and image analysis browse or keyword search through sensing data, existing applications and software that can be used to build tools.

NASA collects petabytes of data each year from its constellation of Earth-orbiting satellites, but both the datasets themselves and the tools for processing them have been spread across dozens of sites, making it difficult for potential users to access and use the data. This new comprehensive collection assembled by NASA's Technology Transfer program offers users an easy way to tap into both near-real-time and archived data and imagery from satellites and aircraft monitoring a wide variety of natural and man-made phenomena. <https://gcn.com>

Remote sensing to deal with national strategic challenges: Iran

Remote sensing centers enjoy great technology for dealing with national strategic challenges like drought, water resources management and crisis management, the Iranian Space Agency (ISA) director said recently. Remote sensing is the process of detecting and monitoring the physical characteristics of an area by measuring its reflected and emitted radiation at a distance from the

targeted area. ISA plans to provide a road map for launching a remote sensing center in the near future. www.tehrantimes.com

Model fuses social media, RS data with goal of identifying nuclear threats

A new computational model allows researchers to draw on normally incompatible data sets, such as satellite imagery and social media posts, to answer questions about what is happening in targeted locations. The researchers developed the model to serve as a tool for identifying violations of nuclear nonproliferation agreements.

“Our goal was to develop a working framework that uses information from a variety of sensors and data sources to identify these potential violations of nuclear nonproliferation,” says Hamid Krim, co-author of a paper on the work, a professor of electrical and computer engineering at North Carolina State University and director of the VISSTA Laboratory.

“Some of these data may be conventional, such as Geiger counter readings or multispectral data from satellite imagery. But many of these data sources may be nontraditional, such as social media posts. And these sources provide a wide variety of data that are not normally compatible, such as the text included on Twitter posts and the images posted on Flickr.

“By making these different inputs compatible with each other, we are able to accept a broader range of data inputs and use that data in a meaningful way that, ultimately, can help authorities reach more reliable conclusions,” Krim says. www.eurekalert.org

China successfully launches 2 remote sensing satellites PRSS-1, PakTES-1A

China has successfully launched two remote sensing satellites for its “all-weather” ally Pakistan. The launch of the two satellites marks yet another space cooperation between China and Pakistan since the launch of PAKSAT-1R, a communication satellite, in August 2011.



8th China Surveying and Mapping Geographic Information Technology Equipment Expo

September 26-28, 2018, Deqing, Zhejiang

Guide: Ministry of Natural Resources of People's Republic of China
China Association for Science and Technology
Host: Chinese Society for Surveying, Mapping and Geoinformation
Co-Organize: Nanjing Tleer Exhibition Co., Ltd

WWW.TLEERW.COM



2018 China (Nanjing) BeiDou Satellite Navigation Application Expo & China (Nanjing) Smart City Expo

GNSS

Nov 30-Dec 2, 2018, Nanjing, China

... WWW.BDSEXPO.COM ...





The satellites — PRSS-1 and PakTES-1A — were launched from the Jiuquan Satellite Launch Centre in northwest China at 11:56 am using a Long March-2C rocket, state-run Xinhua news agency reported. The PRSS-1 is China's first optical remote sensing satellite sold to Pakistan. It is the 17th satellite developed by the China Academy of Space Technology (CAST) for an overseas buyer. A scientific experiment satellite, PakTES-1A, developed by engineers of the Pakistan Space and Upper Atmosphere Research Commission (Suparco), was sent into orbit using the same rocket. www.financialexpress.com


Russia to Procure New Remote-Sensing Satellite

The Russian space agency Roscosmos is planning to issue a manufacturing contract to the Research and Production Association of Machine-Building for a new remote-sensing satellite worth \$147 million.

The sensing satellite will be based on an upgraded new model of the Kondor-FKA S-band radar spacecraft and due for delivery to the customer by November 2025. Once built, Roscosmos will then launch the satellite from the Vostochny spaceport on a Soyuz-2.1a rocket. www.satellitetoday.com

New advancements in high accuracy photogrammetry payload

Insitu, a wholly-owned subsidiary of The Boeing Company has announced it is approaching the theoretical limits of accuracy for photogrammetry through advancements in its High Accuracy Photogrammetry (HAP) capability.

In June, Insitu's latest accuracy improvement prototype validated that its HAP onboard payload now is accurate to within five centimeters (cm) horizontally and 10cm vertically. This marked increase in accuracy is groundbreaking and now leads the industry inaccuracies that can be obtained without ground control from a fixed-wing Unmanned Aerial System (UAS) traveling more than 100km (62.1 miles) per hour from higher than 1,000 ft. 

Virtual Surveyor streamlines workflow

The Virtual Surveyor drone surveying software now offers a faster, more efficient workflow and better overall user experience in a more stable platform. These new capabilities, along with an improved licensing system and an extended free application, are available now in Virtual Surveyor 6.

The software leverages the expertise and interpretation skill of a land surveyor and combines it with the computing power of the computer. It generates an interactive onscreen environment through orthophotos and digital surface models, generated from the UAV, where the surveyor selects survey points and breaklines to define the topography. www.virtual-surveyor.com.

CTSi tests navigation system for GPS-denied UAS navigation

CTSi and partner L3 Technologies completed flight-testing this month of a newly developed integrated communication and navigation system for use in highly contested and GPS-denied environments. Designated the Enhanced Link Navigation System (ELNS), the prototype was built under a U.S. Navy \$8.7 million Small Business Innovative Research (SBIR) Phase III contract. ELNS utilizes L3 Technologies' waveforms that defeat adversary strategies to detect and disrupt allied signals, using waveforms that are essential in communications-denied and GPS-denied environments.

Aeronyde and Unify partnership

Florida-based Autonomous Aerial Systems (AAS) company Aeronyde and Belgian Unmanned Traffic Management provider Unify announced a partnership to bring advanced UAV technology to emergency responders. The companies will integrate Unify's Unmanned Traffic Management services, along with Aeronyde's system for Autonomous flight, to create an efficient self-flying system for police and fire departments. The Aeronyde-Unify partnership will create an autonomous system to enable emergency responders

to scale their drone operations. The resulting system will offer on-demand dispatching of registered and authorized drones, and will deliver real-time situational awareness of scenes of distress. www.unify.aero

Drone-based high-resolution thermal inspection capabilities

Kespry, the leading drone-based aerial intelligence solution provider, has announced new high-resolution thermal inspection capabilities for commercial property and industrial facilities. Thermal inspection solution is based on radiometric temperature analysis, providing actionable data to people inspecting roofs.

Radiometric analysis means that a specific temperature is displayed for a specific point on a roof. In contrast, non-radiometric thermal drone data simply shows general temperature differences and changes in an area, making it hard to determine whether there is a specific point of damage or concern. www.prnewswire.com

Dedrone introduces drone detection in the Cloud

Dedrone Cloud is a new platform that advances Dedrone's offerings, and enables smooth deployment of the its solution, accelerating the process for organizations to develop a threat analysis of their airspace.

Dedrone Cloud streamlines and accelerates drone detection technology installations, without requiring on-site IT infrastructure or maintenance. www.dedrone.com

Crowdfunding campaign for advanced AI-powered drone

Airlango launched Mystic, an advanced AI-powered drone with the ability to recognize and autonomously follow its owner, obey gesture commands from the ground, and take high precision photos without user interaction.

The proprietary technology is the first ever to include neural-computing based

AI functionality and flight control on the same chipset. The company hopes to play a part in ushering in a new era of autonomous robots that serve the needs of users through advanced perception and neural processing. www.prweb.com

Niti Aayog, India expects drones to be instrumental in development

Amitabh Kant, CEO of NITI Aayog, the official policy think tank of the government of India, believes that Unmanned Aircraft Systems (UAS) have the potential to transform many sectors and modernize India at a rapid pace.

Emphasizing that drones are going to replace 80% of the operations presently carried out by the manned aircrafts Kant said that integrating drones in civilian space is a challenging job and would require an appropriate regulatory framework. As India finally prepares itself to allow drones for civilian purposes, the NITI Aayog has asked manufacturers to get

ready for the huge demand that could reach more than \$50 billion in the next 15 years

India's Ministry of Civil Aviation, which came out with a draft drone policy on civilian drones last November, is expected to soon start the registration process of drones.

Enterprise Shield Drone Protection Service Plan

DJI, the world's leader in civilian drones and aerial imaging technology, recently announced DJI Enterprise Shield, a new customizable drone protection service plan designed to meet the diverse needs of today's commercial drone operators. It is the first comprehensive coverage plan of its kind that covers DJI's trusted line of enterprise products, providing broad accident coverage, repair and replacement services, free shipping and rapid delivery, and the option to share coverage across a fleet of enterprise products.

MDA to provide mission-critical sensors for the SPACE DRONE

MDA has announced that a contract was signed between its recently acquired Neptec UK Ltd. (Neptec) company and Effective Space, the UK company pioneering last-mile logistics in space, for the supply of a space flight LIDAR and the infrared camera for its on-orbit servicing SPACE DRONE™ spacecraft.

Capable of extending the life of aging satellites by as many as 15 years, the SPACE DRONE spacecraft uses MDA's LIDAR and infrared camera to confidently and safely approach and dock with orbiting geostationary satellites.

Two SPACE DRONE™ spacecraft will be launched into orbit in 2020, as part of a \$100 million contract with a major regional satellite operator. MDA will execute the project from its newly expanded United Kingdom business. www.prnewswire.com 



GNSS POST-PROCESSING



PRECISION ACROSS THE BOARD

FREE TRIAL > effigis.com/ezsuv



Beidou's third-generation satellite navigation makes a splash

More than 40,000 fishing boats in China have been equipped with receivers tuned to China's Beidou Navigation Satellite System, to provide better search and rescue for ships in trouble, a Beidou expert said. "Fishers call the Beidou system their patron," Yang Yuanxi, an academician with the Chinese Academy of Sciences and deputy chief designer of the system, said recently.

China has 140,000 fishermen whose life on the sea inevitably comes with occasional mishaps, such as extreme weather, collisions or submerged rocks, Mr Yang said. If an accident involves a ship equipped with Beidou receivers, the system can transmit messages for help and pin the precise location for other ships in the vicinity. www.telegraph.co.uk

China launches another BeiDou navigation satellite

China sent a new BeiDou navigation satellite into orbit on a Long March-3A rocket from the Xichang Satellite Launch Center, in the southwestern Sichuan Province on July 10.

The satellite is the 32nd of the BeiDou navigation system, and one of the BeiDou-2 family, which is the second generation of the system.

Safer airport approaches with 3-D satellite-based navigation

BLUEGNSS's focus has been on advancing the adoption of the European global navigation satellite system (GNSS) in Greece, Italy, Cyprus and Malta. The four countries together form the BLUE MED functional airspace block (FAB), airspace in which air traffic is managed irrespective of national boundaries. BLUE MED is one of the nine FABs formed in Europe in order to reduce the fragmentation of the European air traffic network.

Three-dimensional GNSS approaches are being designed for 11 airports in the BLUE

MED FAB: 4 each in Greece and Italy, 2 in Cyprus and 1 in Malta. The primary aim is to harmonise the implementation of required navigation performance approaches among the four countries. This will enable aircraft to fly along precise flight paths with greater accuracy, and will make it possible to pinpoint aircraft position with precision and integrity.

Now close to completion, BLUEGNSS (Promoting EGNSS Operational Adoption in BLUEMED FAB) is the first project of its kind to be coordinated at FAB level. It may serve as a catalyst to spread required navigation performance approach know-how in the region and beyond, to the whole of Europe. www.bluedmed.aero/

Russia plans to launch new Glonass-K2 satellite

Russia is planning to launch a Glonass-K2 satellite under the GLONASS-K series. The launch is expected to be conducted either by a Soyuz-2 carrier rocket from the Plesetsk spaceport in Russia, or by an Angara rocket from the Vostochny cosmodrome in the Russian Far East by 2022. www.aerospace-technology.com

Molecular clock could greatly improve smartphone navigation

MIT researchers have developed the first molecular clock on a chip, which uses the constant, measurable rotation of molecules — when exposed to a certain frequency of electromagnetic radiation — to keep time. The chip could one day significantly improve the accuracy and performance of navigation on smartphones and other consumer devices.

Today's most accurate time-keepers are atomic clocks. These clocks rely on the steady resonance of atoms, when exposed to a specific frequency, to measure exactly one second. Several such clocks are installed in all GPS satellites. By "trilaterating" time signals broadcast from these satellites — a technique like triangulation, that uses 3-D dimensional data for positioning — your smartphone and other ground receivers

can pinpoint their own location. But atomic clocks are large and expensive. Your smartphone, therefore, has a much less accurate internal clock that relies on three satellite signals to navigate and can still calculate wrong locations.

Researchers from MIT's Department of Electrical Engineering and Computer Science (EECS) and Terahertz Integrated Electronics Group have now built an on-chip clock that exposes specific molecules — not atoms — to an exact, ultrahigh frequency that causes them to spin. When the molecular rotations cause maximum energy absorption, a periodic output is clocked — in this case, a second. As with the resonance of atoms, this spin is reliably constant enough that it can serve as a precise timing reference. In experiments, the molecular clock averaged an error under 1 microsecond per hour, comparable to miniature atomic clocks and 10,000 times more stable than the crystal-oscillator clocks in smartphones. Because the clock is fully electronic and doesn't require bulky, power-hungry components used to insulate and excite the atoms, it is manufactured with the low-cost, complementary metal-oxide-semiconductor (CMOS) integrated circuit technology used to make all smartphone chips. <http://news.mit.edu>

A \$225 GPS spoofer can send sat-nav-guided vehicles into oncoming traffic

Billions of people—and a growing number of autonomous vehicles—rely on mobile navigation services from Google, Uber, and others to provide real-time driving directions. A new proof-of-concept attack demonstrates how hackers could inconspicuously steer a targeted automobile to the wrong destination or, worse, endanger passengers by sending them down the wrong way of a one-way road.

The attack starts with a \$225 piece of hardware that's planted in or underneath the targeted vehicle that spoofs the radio signals used by civilian GPS services. It then uses algorithms to plot a fake "ghost route" that mimics the turn-by-turn navigation directions contained in the

original route. Depending on the hackers' ultimate motivations, the attack can be used to divert an emergency vehicle or a specific passenger to an unintended location or to follow an unsafe route. The attack works best in urban areas the driver doesn't know well, and it assumes hackers have a general idea of the vehicle's intended destination. <https://arstechnica.com>

U.K. to EU: Time Is Running Out for Deal on Galileo Satellites

The EU has effectively ruled out British companies bidding on new contracts for the 10 billion-euro (\$11.6 billion) program, and also says it will exclude Britain from the Public Regulated Service -- the encrypted navigation signals used for government and defense purposes. That's despite U.K. units of Airbus SE and CGI Group Inc. carrying out extensive work on the program since its inception.

"We are not yet past the point of no return, but time is running out," Gyimah told a House of Lords Committee on Thursday. "We've also made it clear

that any gap in U.K. involvement in the design and development of Galileo, the PRS, would also mean the U.K. could not rely on the system for our own national security interests."


Galileo has become one of the surprise flash-points of Britain's negotiations to leave the EU, and emphasizes the gap in negotiating stances. The EU is sticking to its rulebook, which says Britain should be treated as any other third nation after Brexit, while British officials argue the country's close involvement in the program to date means it should have privileged access. Britain has said that it'll work on its own satellite array -- possibly in conjunction with countries such as Australia -- if it can't have the access it wants to the EU program. At the same time, ministers have taken offense at the idea the U.K. can't be trusted to stay involved in the secure signal program.

"The very idea that somehow the U.K. cannot be trusted on security matters is for the birds," Gyimah said. www.bloomberg.com

£100mn to study rival EU Galileo space program

Having faced an onslaught of requests to loosen the purse strings for the Ministry of Defense (MoD), Philip Hammond is now under pressure to cough up £100 million for a study into a UK rival to the EU's Galileo satellite.

Chancellor of the Exchequer Hammond received the request last week from Business Secretary Greg Clark, who suggested that the funds be released to conduct a two-year feasibility study into a British satellite navigation system similar to the EU's Galileo program.

The request comes as the EU continues to deny the UK access to the Galileo program after it leaves the bloc in March 2019. Launched in 2003 as the first civil-run satellite navigation system and an independent rival to the US GPS, the UK had invested €1.4 billion (\$1.65bn) of the €10 billion (\$11.8bn) spent to fund Galileo. www.rt.com 

LINERTEC

Linertec, your Benefit in Surveying and Construction

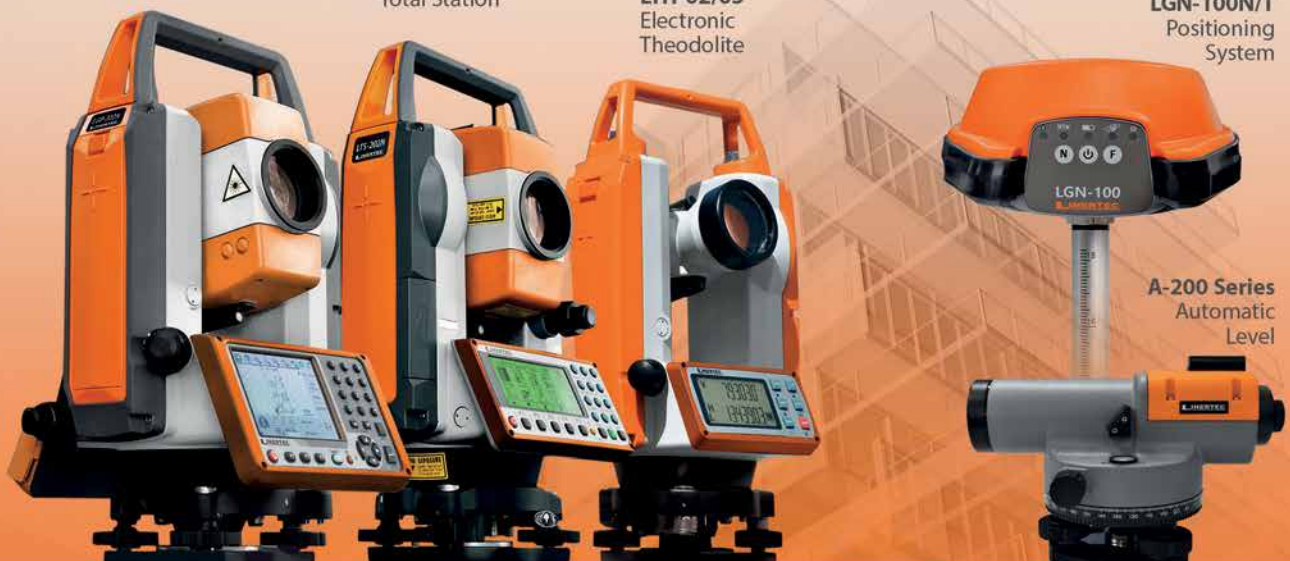
The Linertec Precision Instruments are designed and developed in Japan. They are the result of our long-established expertise in Surveying and Construction.

LGP-300 Series
WinCE Reflectorless
Total Station

LTS-200 Series
Reflectorless
Total Station

LTH-02/05
Electronic
Theodolite

LGN-100N/T
Positioning
System



A-200 Series
Automatic
Level

Ordnance Survey to help Guyana reap the benefit of geospatial data

Ordnance Survey (OS) is to provide consultancy services to the Guyana Lands and Surveys Commission (GLSC) to re-establish and further develop the GPS Continuously Operating Reference Stations (CORS) network in Guyana. The project seeks to establish and sustainably maintain a modern, robust and accurate national geodetic positioning network for Guyana. A re-established CORS network will help Guyana in relation to meeting its Sustainable Development Goals (SDGs) and will enable better transport, secure land tenure, better government, increased economy and happier citizens.

OS, working with GLSC, will establish full functionality and usability of the existing Network Operations Centre (NOC) and 8-site CORS network. Design and document associated CORS management processes and train staff to be able to operate all first and second line operational activities, establish third line support cover with GNSS equipment and software manufacturer. OS will assist GLSC in specifying, procuring and deploying specialist equipment for the CORS network in accordance with identified national development needs and the strategic business requirements of GLSC.

DARPA explores underground mapping

The Defense Department's research arm is getting interested in mapping and navigating subterranean space.

As part of its SubT Challenge, the Defense Advanced Research Projects Agency wants technologies to help the military and responders map, navigate and search underground complexes, from man-made tunnel systems, urban and municipal underground infrastructure as well as natural cave networks.

DARPA will convene a competitor's day in the Louisville Mega Cavern, a 100-acre manmade limestone cave underneath a portion of the city's southern section. The cave currently houses commercial

storage facilities and public recreation businesses such as underground zip lines and electric bike and tram tours. Before being converted to current uses in the late 1980s, the cavern was an underground crushed limestone quarry from the 1930s to the 1970s.

DARPA said it is looking for teams of providers that can put together core systems that have autonomy, perception, networking and mobility with an eye towards developing integrated systems and software solutions that can meet the extreme challenges underground environments present. <https://gcn.com>

Blockchain-based open mapping architecture

Hyperion, an open blockchain-based mapping architecture based on Hyperion Digital Location Right (HDLR), has announced the official launch of its mapping technology. It fundamentally disrupt existing mapping systems by providing the infrastructure to support a completely decentralized, self-governing global map that users anywhere can contribute to, edit or utilize for their own needs, and share the economic value.

The Hyperion ecosystem addresses a number of key pain points in mapping development. First, the cost of developing and maintaining detailed, up-to-date maps using a top-down model is hugely expensive and inefficient. Second, this model makes it difficult to ensure that maps are accurate or up-to-date. Third, current mapping infrastructure is controlled by governments or private companies, creating barriers for other users to access or utilize these maps. Hyperion addresses this using a three-stranded model which it calls the 'Hyperion Trinity'. www.hyn.space

Singapore startup wants to help 'Bricks' target audience via location

Despite the rise of e-commerce marketplaces, traditional retail players still can compete successfully if they have the right tools to better target consumers in the physical realm. This is where Singapore startup WhereIsWhere hopes to step in

and offer location-based services, which it says will plug a critical hole in the industry and arm brick-and-mortar retailers with the ability to engage potential customers.

According to the CEO and founder Terence Mak, every merchant was eager to tell potential customers the promotions it offered, but the information business owners could provide was limited to what could be displayed on the storefront. This form of marketing to capture passerby traffic was no longer effective adding instead that mobile now was the new consumer interface.

Azteca Systems releases Cityworks 15.3

Cityworks-Azteca Systems announced the release of Cityworks 15.3, the latest version of the company's web GIS-centric platform for public asset management. The new release features significant enhancements to support apps that streamline the care of public infrastructure, permitting, and property.

It is designed to help organizations manage public assets and their associated data, work activities, and business processes. This release supports end user functionality in Cityworks apps such as Performance Budgeting, Public Access, Operational Insights, and Storeroom. It also supports the release of Style 1.0, which allows users to customize the interface of other apps for their end users. www.cityworks.com

Australia to spend \$7bn on six drones

A new partnership with the US Navy will see Australian defence purchase a fleet of long range Triton drones for maritime surveillance of the waters surrounding Australia's continental border and the Asia-Pacific region, with the first system to be delivered in 2023.

It is reported that the estimated cost of the entire fleet and associated infrastructure will total almost \$7 billion, with the Government's investment in the first of these six aircraft coming in at a cost of \$1.4 billion. www.spatialsource.com.au

Luciad's V2018.0 released

Luciad's V2018.0 release, empowers users to create a Smart Digital Reality by enabling the streaming of highly detailed point cloud data to both the desktop and the browser, and by giving users the ability to develop and utilize intricately detailed 3D reality meshes. These features will be available in Luciad Lightspeed and LuciadRIA, Luciad's modular and customizable solutions for geospatial awareness on the desktop and in the browser. LucadFusion, the all-in-one server solution for geospatial data publication and management can now manage vast amounts of point cloud and 3D reality mesh files, index them and stream them using open standards.

HxGN SmartNet, AZGPS to expand GNSS correction services in US

HxGN SmartNet has partnered with AZGPS LLC to expand access to quality network correction services for GNSS users in the southwestern US. It is, a high-precision, high-availability GNSS network correction service provided by Hexagon's Geosystems division. AZGPS, based in Florence, Arizona, serves professionals across Southern California and Arizona

NovAtel's GNSS+INS combined system with SPAN technology

NovAtel has announced that it is now delivering their market-leading SPAN® tightly-coupled GNSS+INS navigation technology in a rugged, ultra-compact unit. Commercially exportable and ideal for integration into a wide variety of applications, the high-performance SPAN CPT7 is designed to deliver assured positioning – anywhere, in a package one-quarter the size of the highly successful SPAN-CPT.

Leading-edge SPAN technology leverages generations of precise positioning expertise and the most advanced algorithms to tightly-couple GNSS and INS measurements. This system enables continuous, robust positioning and fast reacquisition in challenging navigation environments where GNSS signals may be unreliable or unavailable for short periods.

Rockwell Collins and Iridium partnership

Iridium Communications Inc. has announced Rockwell Collins as the newest Iridium Certus service provider for the aviation industry. Rockwell Collins will be adding the service to its comprehensive suite of aircraft connectivity applications for commercial, government and ARINC DirectSM business customers.

Iridium Certus will bring broadband functionality, with enterprise-grade quality of service, to the aviation industry no matter where in the world an aircraft may fly. The service will soon deliver the fastest L-band broadband speeds on the market at a competitive price with industry-leading small form factor antennas and terminals. The Iridium Certus high-gain antenna (HGA) solutions will provide data speed options of up to 704 Kbps, and eventually as high as approximately 1.4 Mbps following full Iridium® NEXT deployment, with an antenna size of approximately 24 x 10 x 6cm, while the low-gain antenna (LGA) solutions will enable data speeds of up to 176 Kbps. www.IridiumNEXT.com

ComNav Technology wins biggest RTK tender

ComNav Technology, in cooperation with its local Indonesian distributor, has successfully won the biggest RTK tender, which was organised by The Ministry of Agrarian Affairs and Spatial Planning/ National Land Agency of Indonesia, for 1,046 sets of SinoGNSS T300 GNSS receivers. According to the National Land Agency information, the RTK products will be used in Indonesian cadastral surveying projects. The transaction renewed the record since GNSS RTK products were innovated.

Tallysman GNSS antenna designed for precision positioning

GNSS antenna maker Tallysman has introduced the TW7875 magnetic mount GNSS antenna, which is designed for precision dual-frequency positioning. It is capable of receiving GPS L1/L5, GLONASS G1, BeiDou B1, Galileo E1/E5a and NavIC L5.


Military precision navigation capabilities to commercial markets

The HGuide n580 is the first Honeywell-produced, industrial-focused navigation solution that uses both precision inertial measurement unit technology and GNSS to improve location accuracy even when facing natural and manmade obstacles. Roughly the size of a deck of cards, the HGuide n580 gives Honeywell's industrial customers the capabilities needed to navigate accurately in areas with limited satellite coverage, such as densely populated cities where tall buildings, underground tunnels, and multi-layer freeway stacks or bridges often create challenges to traditional GPS navigation.

EN-150 Precision Fiber Optic Gyro-Based Inertial Measurement Unit

EMCORE Corporation has announced the introduction of its new EN-150 Inertial Measurement/Navigation Unit for unmanned aerial vehicles, dismounted soldiers and weaponry, platform stabilization and applications where GPS is unavailable. Designed with options for full navigation, or as a higher performance, smaller size replacement for Ring Laser (RLG) Inertial Measurement Units (IMUs), the EMCORE EN-150 is the smallest, most affordable Fiber Optic Gyro (FOG)-based IMU available today at its performance level. www.emcore.com

Intermap Technologies introduces NEXTMap One

NEXTMap One offers precision, 3D geospatial data at an unprecedented 1-m resolution anywhere in the world. It is available as either digital surface models (DSM) or bare earth digital terrain models (DTM), is produced using Intermap's patented Intelligent Resolution Improvement System (IRIS™) and represents a technological advancement in global elevation data production. By combining the best features from multiple sensors, IRIS generates a seamless global dataset that is both highly accurate and spatially rich. Intermap uses high-resolution satellite imagery along with multi-band radar, LiDAR and other datasets to produce NEXTMap One .

Galileo update

Galileo quartet successfully launched from Kourou

Four new Galileo satellites were successfully launched from the European spaceport in Kourou, French Guiana on July 25, bringing the constellation to a total of 26 satellites.

For the second time, the European GNSS Agency (GSA) is responsible for the Early Orbit Phase (EOP) of this mission, overseeing Spaceopal - a joint venture between Telespazio and DLR-GfR - in their role as Galileo Service Operator (GSOp) and EOP Mission Director, and CNES as EOP Operations Director. The EOP is one of the most important phases of a space mission during which the spacecraft is launched and put into the correct orbit and the first satellite elements are gradually switched on and tested.

“Today is an excellent opportunity to celebrate what Europe can achieve when resources, competences and commitments are brought together,” GSA Executive Director Carlo des Dorides said immediately after the launch. “Yet the success of Galileo is not measured by the number of satellites, but by the number of users, and here too we have achieved remarkable results. In the past 18 months, Galileo has moved from zero to 400 million users,” he said. www.gsa.europa.eu

Galileo satellites viewed in smartphone app

ESA ran an internal competition for its trainees to develop an app capable of making positioning fixes using only Galileo satellites.

“As part of our support for the competition, we developed our own

app on a voluntary basis to serve as a benchmark,” explains Paolo Crosta of ESA’s Radio Navigation Systems and Technology section. “We included this augmented reality view, so users can ‘see’ the satellites their smartphone is using as they hold it up to the sky.”

The positioning calculations and assistance data functions for the app were developed by Paolo, with telecom engineer Tim Watterton contributing the main structure of the app, together with how it looks and its user interface.

Tim adds: “The satellites are overlaid in real time on the camera view in their predicted positions in the sky, based on ‘ephemeris’ information, assistance data that describes the current satellite orbits with high precision.

“When a signal is being received, the satellite is shown in green, overlaying the predicted position. The satellite shown in red is one of the two placed in elongated orbits, but these satellites are expected to be used soon in the operational constellation. Satellites coloured orange are transmitting, but the signal is not detected, which may be due to obstruction by terrain or buildings.”

Panning the phone around to position the crosshair over a green coloured satellite adds additional information about it, such as its signal status, ‘pseudo-range’ (the uncorrected distance the signal has travelled to reach the receiver) plus the satellite’s manufacturer, launch date among other items. <https://phys.org/news/2018-07-galileo-satellites-viewed-smartphone-app.html#jCp> ▽

Singapore’s first 5G pilot network

Singtel and Ericsson are strengthening their 5G Centre of Excellence Programme partnership with the announcement of a new initiative that will see Singapore’s first 5G pilot network go live this year.

Using Ericsson’s 3GPP standards-compliant 5G technology with the trial spectrum allocated by Singapore’s Info-Communications Media Development Authority (IMDA), the pilot network will deliver 5G coverage with enhanced Mobile Broadband (eMBB) speed and low latency communications. www.ericsson.com

Arcules launches Intelligent Video Cloud platform

Arcules, the provider of video cloud internet of things (IoT) as a service technology, announced the launch of the Arcules platform at Google Cloud Next. The Arcules Intelligent Video Cloud platform aggregates and analyzes previously untapped video surveillance and IoT sensor data, identifies trends in that data and applies predictive analytics to help businesses optimize operations and improve safety. Using the Arcules solution, businesses can access these insights anywhere and from any device in a streamlined, centralized platform, and quickly scale the solution without the burden of additional maintenance or hardware.

Intel and SiTime collaboration

SiTime Corporation, provider of MEMS timing, and Intel announced a collaboration to work together on integrating timing solutions for Intel’s 5G multi-mode radio modems, with additional applicability to Intel LTE, millimeter-wave wireless, Wi-Fi, Bluetooth, and GNSS solutions.

SiTime’s MEMS timing solutions enhance system performance in the presence of stressors such as vibration, high temperature, and rapid thermal transients. Such stressors can disrupt the timing signal and result in network reliability issues, lower data throughput, and even connectivity. <https://newsroom.intel.com>



Uber halts autonomous car program, lays off 100 operators

Uber's experimentation with self-driving cars are being put on the backburner for now, and consequently, it has led to a lay off in the San Francisco Bay area.

Recently, the ride-sharing company laid off around 100 autonomous-vehicle operators in the wake of an accident in March in which an Uber self-driving car collided with a pedestrian in Tempe, Arizona. www.cnn.com

Baraja unveils Spectrum-Scan LiDAR for autonomous vehicles

Sydney-based company Baraja has publicly unveiled Spectrum-Scan LiDAR, which uses prism-like optics and shifting wavelengths of light to create powerful eyes for autonomous vehicles, giving those vehicles unprecedented data and clarity of vision, a requirement for safe, fully-autonomous driving. www.roadtraffic-technology.com

Vietnamese transport ministry allows autonomous car development

Vietnam's Ministry of Transport supports the development of self-driving cars because it is in line with the government's strategy on the fourth industrial revolution development. The ministry in Hanoi has positively responded to a proposal by a local technology firm named FPT Software on allowing it to operate its driverless cars on a trial basis on the internal road in a hi-tech park in Ho Chi Minh City. www.xinhuanet.com

Baidu Joins Forces with Softbank's SB Drive, King Long

Baidu, Inc. SB Drive, a subsidiary of Softbank dedicated to self-driving technology research, and King Long, a leading commercial vehicle manufacturer in China, has announced a strategic partnership to jointly develop and deploy a version of the Apolong self-driving mini bus for the Japanese market. Under the agreement, ten Apolong mini buses

will be exported to Japan from China in early 2019. This agreement marks the first time autonomous vehicles will be exported from China.

New autonomous vehicle platform connects road authorities with vehicle operators

Highly automated vehicles (HAV) are currently testing on public roads in fewer than 50 cities around the world, but more markets are interested in bringing this new technology to their streets. INRIX has announced a new platform that provides the foundation for cities and road authorities to communicate with operators for safe and effective deployment of HAVs on public roads. INRIX AV Road Rules is the first platform that enables cities and road authorities to assign, validate and manage traffic rules and restrictions for autonomous vehicles operating on public roads. The platform also leverages information from HAVs to report infrastructure improvement needs, making the roads safer for all users. www.prnewswire.com



UC'18

Discover how GIS is inspiring what's next.

4 Sept
2018

Kolkata
Hyatt Regency

6 Sept
2018

Hyderabad
The Park


10-11 Sept
2018

Delhi NCR
The Leela Ambience Gurugram

Register today

 esriindia.com/indiauc

 register@esriindia.com

 +91 120 428 5935

Follow Esri India:

 facebook.com/esriindia

 twitter.com/esriindia

 linkedin.com/company/esriindia



Scan to Register

SUBSCRIPTION FORM

YES! I want my **Coordinates**

I would like to subscribe for (tick one)

1 year 2 years 3 years

12 issues 24 issues 36 issues

Rs.1800/US\$100 Rs.3000/US\$170 Rs.4300/US\$240

**SUPER
saver**

First name

Last name

Designation

Organization

Address

.....

City Pincode

State Country

Phone

Fax

Email

I enclose cheque no.

drawn on

date towards subscription

charges for Coordinates magazine

in favour of 'Coordinates Media Pvt. Ltd.'

Sign Date

Mail this form with payment to:

Coordinates
A 002, Mansara Apartments
C 9, Vasundhara Enclave
Delhi 110 096, India.

If you'd like an invoice before sending your payment, you may either send us this completed subscription form or send us a request for an invoice at iwant@mycoordinates.org

MARK YOUR CALENDAR

September 2018

Esri India User Conference 2018

September 4 Kolkata
September 6 Hyderabad
September 10 -11 Delhi NCR
www.esriindia.com/events/2018/uc

Inter Drone 2018

5 - 7 September
Las Vegas, USA
www.interdrone.com

Smart Geospatial Expo

12 -14 September 2018
Seoul, Korea
www.smartgeoexpo.kr

EuroGEOSS Workshop

12 - 14 September
Geneva, Switzerland
<https://ec.europa.eu>

Africa GEO

17 - 19 September
Johannesburg, South Africa
<https://africageo.org.za>

INSPIRE Conference 2018

18 - 21 September
Antwerp, Belgium
www.inspire.ec.europa.eu/conference2018

5th EARSeL Joint Workshop "Urban Remote Sensing – Challenges & Solutions"

24 - 26 September
Dortmund, Germany
<http://urs.earsel.org>

International Symposium and Workshop on A smart sustainable future for all

24 - 26 September
Melbourne, Australia
ssf2018.com

ION GNSS+ 2018

24 - 28 September
Miami, USA
www.ion.org

The 8th China Surveying and Mapping GI Tech Equipment Expo

26 - 28 September
Deqing, Zhejiang, PR China
www.tleerw.com/en/

October 2018

Joint Geo Delft Conference

The 6th International FIG 3D Cadastre Workshop

The 3D Geoinfo Conference

1- 5 October
Delft, the Netherlands
www.tudelft.nl/geodelft2018

39th Asian Conference on Remote Sensing (ACRS 2018)

15 - 19 October
Kuala Lumpur, Malaysia
<http://acrs2018.mrsa.gov>

Intergeo 2018

17 - 18 October
Frankfurt, Germany
www.intergeo.de

November 2018

Trimble Dimensions 2018

5 - 7 November
Las Vegas, USA
www.trimbledimensions.com

CHINTERGEO2018

7 - 9 November
Chengdu, Sichuan Province
PR China
www.chintergeo.com

International Navigation Conference 2018

12 - 15 November
Bristol, UK
www.rin.org.uk

ITSNT 2018

13 - 16 November
Toulouse, France
www.itsnt.fr

Commercial UAV Show

14 - 15 November 2018
London, UK
www.terrapinn.com/exhibition/the-commercial-uav-show/

United Nations World Geospatial Information Congress

19 - 21 November
Deqing, China
www.unwgic2018.org

International Symposium on GNSS (ISGNSS 2018)

21 - 23 November
Bali, Indonesia
www.isgnss2018.com

CHINTERGEO 2018

November
ChengDu, PR China
www.chintergeo.com/en/index.html

The Pacific GIS and Remote Sensing User Conference

26 - 30 November 2018
SUVA, Fiji
www.picgisrs.org

The 16th IAIN World Congress 2018

28 November – 1 December
Chiba, Japan
<https://iain2018.org>

BeiDou Satellite Navigation Application Expo & Smart City Expo

30 November - 02 December
Nanjing, PR China
www.tleer.cn/enbdsexpo



Trimble

DIMENSIONS



LEAD YOUR BUSINESS INTO TOMORROW

Experience the 2018 Trimble Dimensions User Conference—three action-packed days to witness how technology is transforming the way we work. Be inspired by visionary speakers. Take part in useful hands-on workshops and breakout sessions. Get excited with game-changing innovations at our interactive expo made to move you and your business forward. Network with thousands of your professional peers.

November 5-7, 2018 at The Venetian in Las Vegas, Nevada.

TrimbleDimensions.com



NT1066 ^{NEW}

Multi-Channel GNSS RF Front-End IC

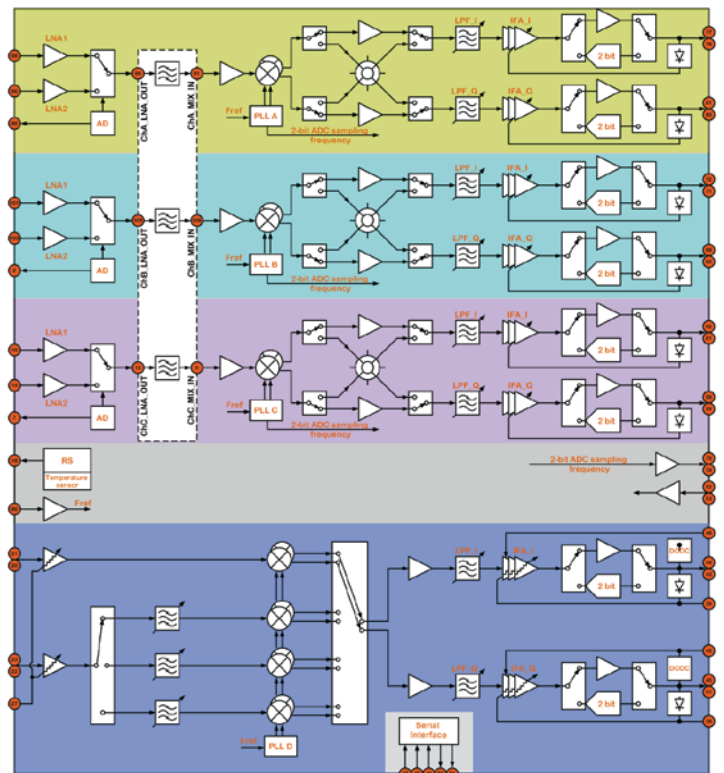
*Precision is going to be
simpler, cheaper, faster ...*

NT1066 is a multi-channel GNSS RF Front-End chip for professional navigation market: geodesy, driverless cars, drones, transport tracking and similar applications.

Product features:

- simultaneous reception of NavIC/ GPS/GLONASS/Galileo/BeiDou/QZSS signals;
- frequency bands: **S**/L1/L2/L3/**L5**/E1/E5/E6/B1/B2/B3:
 - channels "A", "B" and "C" are designed with single conversion low-IF architecture, individually programmable and intended to receive L1, E1, B1, E6, B3, L2, L3, B2, **L5**, E5 in various combinations;
 - channel "D" is dedicated to operate on **S** band of NavIC or L2, L3, **L5** bands of other GNSS and has zero-IF architecture;
- it is possible to eliminate effectively ionospheric distortion utilizing large signal base of NavIC between **L5** and **S** bands;
- full programmability of each of 4 channels (signal bandwidth, downconversion sideband, AGC options, analog/2-bit digitized output, etc.);
- simple and easy-to-use register map for chip configuration.

NT1066 is produced using 0.18 μ m SiGe BiCMOS technology and it is already in mass production.



नाविक के सभी बैंडों के लिए उपयुक्त

अपॉर्टेबल एंड हाई फ्रिक्वेंसी ऑफ नॉन-ए

